

QATAR UNIVERSITY

COLLEGE OF ENGINEERING

RELATING REPRESENTATIVE ELEMENTARY VOLUME OF TORTUOSITY TO
THAT OF POROSITY AS REVEALED FROM COMPUTED TOMOGRAPHY IMAGES

BY

REEM JAMIL AZZAM

A Thesis Submitted to
the Faculty of the College of Engineering
in Partial Fulfillment of the Requirements for the Degree of
Masters of Science in Environmental Engineering

June 2019

© 2019. Reem Azzam. All Rights Reserved.

COMMITTEE PAGE

The members of the Committee approve the Thesis of
Reem Azzam defended on 17/04/2019.

Dr. Riyadh Al-Raoush
Thesis/Dissertation Supervisor

Dr. Ibrahim Abu-reesh
Committee Member

Approved:

Abdel Magid Hamouda , Dean, College of Engineering

ABSTRACT

AZZAM, REEM, J., Masters : June : [2019],

Masters of Science in Environmental Engineering

Title: RELATING REPRESENTATIVE ELEMENTARY VOLUME OF TORTUOSITY TO THAT OF POROSITY AS REVEALED FROM COMPUTED TOMOGRAPHY IMAGES

Supervisor of Thesis: Riyadh, I, Al-Raoush.

Tortuosity and porosity are significant micro-scale parameters that have a major impact on many environmental processes and engineering applications that are usually implemented at a macroscopic scale. Thus, it is essential to quantify the corresponding representative elementary volume of these micro-scale properties to study and improve the understanding of different environmental applications, such as flow and transport of contaminants in porous media systems. 3D x-ray microtomography images of sand systems that have different sizes and geometry were used to compute two important microscopic properties such as porosity and tortuosity. Corresponding representative elementary volumes (REV) of these systems were computed by developing an efficient algorithm using Matlab. Representative elementary volume (REV) of tortuosity was related to that of porosity for each system, to determine whether an REV for porosity is sufficient to define REV for tortuosity. Findings revealed that for regular particles geometry REV_{min} of porosity was less than REV_{min} of tortuosity. However, for irregular particles geometry, the REV_{min} of porosity and REV_{min} of tortuosity were similar. This indicates that REV_{min} value of porosity depends on the geometry and the structure of the porous media. Whereas, REV_{min} value of tortuosity is not affected by the geometry. In addition, the number of particles required to reach REV region was

found to be an easier method to be reflected upon.

ABSTRACT (IN ARABIC)

يعد التعرج والمسامية من الخصائص ذات تأثير كبير على العديد من العمليات البيئية والتطبيقات الهندسية. ليتم تطبيق هذه الخصائص على نطاق التطبيقات والعمليات الهندسية، لابد من إيجاد الحجم التمثيلي لهذه الخواص التي تعتبر صغيرة الحجم، وذلك لدراسة وتحسين فهم التطبيقات البيئية المختلفة، مثل نقل تلوث المياه الجوفية في الوسائط المسامية ونشر الغازات في بنية الوسائط المسامية المعقدة. تتمثل الأهداف الرئيسية لهذه الأطروحة في استخدام الصور المجهرية ثلاثية الأبعاد لخمسة عشر نظاما كل نظام يتسم باختلاف شكل الجزيئات واختلاف أقطارها وذلك لحساب خواص مجهرية مهمة مثل المسامية والتعرج على نطاق واسع. من خلال تطوير خوارزمية فعالة باستخدام برنامج MatLab وذلك للعثور على الحجم التمثيلي للمسامية والتعرج وإيجاد علاقة بينهم. بالإضافة إلى ذلك، تحديد ما إذا كان الحجم التمثيلي للمسامية كافية لتعريف الحجم التمثيلي للتعرج. كشفت النتائج أنه بالنسبة للجزيئات ذات الشكل المنتظمة فإن الحجم التمثيلي للمسامية أقل من الحجم التمثيلي للتعرج. في المقابل بالنسبة للجزيئات غير منتظمة الشكل فإن الحجم التمثيلي للمسامية كان مساويا للحجم التمثيلي للتعرج. بمعنى آخر، تتأثر قيمة الحجم التمثيلي للمسامية بالهندسة وبنية وسائط المسام. بينما، لا تتأثر قيمة الحجم التمثيلي للتعرج بالهندسة وبنية وسائط المسام. بالإضافة إلى ذلك، تم العثور على عدد الجسيمات المطلوبة للوصول إلى وحدة الحجم التمثيلي.

DEDICATION

This thesis is dedicated to my beloved family who has provided me with continuous support and motivation throughout the two years of my Master's study.

ACKNOWLEDGMENTS

Funding was provided by NPRP grant # NPRP8-594-2-244 from Qatar National Research Fund (a member of Qatar Foundation). Moreover, I would like to acknowledge and express my gratitude to my supervisor Dr. Riyadh Al-Raoush for his useful comments; guidance and expert advice have been invaluable throughout all stages of the work. Furthermore, I would also wish to express my gratitude to Eng. Safna Nishad and Eng. Jamal Hannun as they guided me and help me with Matlab software.

A very special gratitude goes out to my parents who have provided me through moral and emotional support in my life. Moreover, I am also grateful to my cousins and friends who have supported me along the way. Without their support, it is impossible for me to finish my graduate education seamlessly.

TABLE OF CONTENTS

DEDICATION	vi
ACKNOWLEDGMENTS	vii
LIST OF TABLES	x
LIST OF FIGURES	xi
CHAPTER 1: INTRODUCTION	1
1.1 Objectives.....	6
1.2 Thesis Organization.....	7
CHAPTER 2: BACKGROUND AND LITERATURE REVIEW	8
2.1 Microscopic properties	9
2.2 Representative elementary volume (REV).....	10
CHAPTER 3: METHODOLOGY	19
3.1 Data	19
3.2 Synchrotron micro-computed tomography	23
3.3 Computation of tortuosity	23
3.4 Calculation of representative elementary volume (REV)	25
3.5 Data Analysis	27
3.5.1 Constructing distributions curves of porosity and tortuosity.....	27
3.5.2 Computing REVmin for porosity and tortuosity	29
CHAPTER 4: RESULTS AND DISCUSSION.....	33

CHAPTER 5: CONCLUSION AND RECOMMENDATION	51
REFERENCES	52
APPENDIX.....	68
Appendix A: Tables for porosity and tortuosity values	68
Appendix B: distribution curves for porosity and tortuosity	73
Appendix C: REVmin Matlab code	81

LIST OF TABLES

Table 1. Physical Properties of the Porous Media Including Porosity, Mesh Size Distribution, D_{50} , Sphericity, and Roundness [12].	22
Table 2. Porosity and Tortuosity Values of all systems.....	25
Table 3. Sub-Volumes Selected Inside The 3D Micro-Computed Tomography Images for REV Analysis.	27
Table 4. REVmin Volume Values of Porosity and Tortuosity for All Systems.....	41
Table 5. REVmin normalized Volume Values of Porosity and Tortuosity for All Systems.	46

LIST OF FIGURES

Figure 1. Microscopic cross section image of a porous medium showing both actual pathway and straight pathway traveled by a molecule.	1
Figure 2. Microscopic cross section image of a porous medium showing solid space and void space.....	3
Figure 3. Schematic diagram of a change of a given material property over the change of volume.	5
Figure 4. (a) Cross-sectional image of system 1 with silica particles geometry, (b) Cross-sectional image of system 7 with quartz particles geometry, (c) Cross-sectional image of system 13 with silica and quartz mixed particles geometry, (d) 3D image of system 1 with silica particles geometry, (e) 3D image of system 7 with quartz particles geometry, and (f) 3D image of system 13 with silica and quartz mixed particles geometry.	20
Figure 5. 3D images showing the subvolume selected for REV analysis.	26
Figure 6. Porosity and tortuosity distribution curve of system 1.....	28
Figure 7. Porosity and tortuosity distribution curve of system 7.....	28
Figure 8. Porosity and tortuosity distribution curve of system 15.....	29
Figure 9. Flow chart of REVmin code.....	31
Figure 10. Using the distribution curve of system_5 as an example to clarify the idea of continuous smooth REV region.	32
Figure 11. Distribution curve of porosity and tortuosity for system 1 marked with the REVmin values of both properties.....	33
Figure 12. Distribution curve of porosity and tortuosity for system 2 marked with the REVmin values of both properties.	33

Figure 13. Distribution curve of porosity and tortuosity for system 3 marked with the REVmin values of both properties.....	34
Figure 14. Distribution curve of porosity and tortuosity for system 4 marked with the REVmin values of both properties.....	34
Figure 15. Distribution curve of porosity and tortuosity for system 5 marked with the REVmin values of both properties.....	35
Figure 16. Distribution curve of porosity and tortuosity for system 6 marked with the REVmin values of both properties.....	35
Figure 17. Distribution curve of porosity and tortuosity for system 7 marked with the REVmin values of both properties.....	36
Figure 18. Distribution curve of porosity and tortuosity for system 8 marked with the REVmin values of both properties.....	36
Figure 19. Distribution curve of porosity and tortuosity for system 9 marked with the REVmin values of both properties.....	37
Figure 20. Distribution curve of porosity and tortuosity for system 10 marked with the REVmin values of both properties.....	37
Figure 21. Distribution curve of porosity and tortuosity for system 11 marked with the REVmin values of both properties.....	38
Figure 22. Distribution curve of porosity and tortuosity for system 12 marked with the REVmin values of both properties.....	38
Figure 23. Distribution curve of porosity and tortuosity for system 13 marked with the REVmin values of both properties.....	39
Figure 24. Distribution curve of porosity and tortuosity for system 14 marked with the REVmin values of both properties.....	39

Figure 25. Distribution curve of porosity and tortuosity for system 15 marked with the REVmin values of both properties.....	40
Figure 26. REVmin volume values of all systems (1-15) for both microscopic properties.....	42
Figure 27. REVmin values for all systems (1-15) of both microscopic properties.	43
Figure 28. Showing pore space and pore particales of (a) 3D image of system 1 with silica particles geometry, and (b) 3D image of system 7 with quartz particles geometry.	45
Figure 29. REVmin normalized volume values of all systems (1-15) for both microscopic properties.	47
Figure 30. REVmin values for all systems (1-15) of both microscopic properties.	48

CHAPTER 1: INTRODUCTION

Tortuosity is considered one of the significant parameters that significantly influence the flow and transport characteristics of porous media. For instance, studying the tortuosity of granular porous media is important because it provides a clear understanding of how contaminated water flows through porous media and therefore, this will aid in designing remediation scheme [1,2]. For instance, CO₂ sequestration describes the long-term storage of carbon dioxide avoided to migrate for the purpose of reducing the amount of greenhouse gases in the atmosphere, which affects climate change that consequently contributes to global warming. Moreover, the amount of produced hydrocarbon is determined from the amount of trapped oil or gas in porous media [3,4]. Hence, it generally influences all mass transfer processes in the field of marine geophysics and geochemistry [5]. Scientifically and from a hydrodynamic point of view, tortuosity is defined as the ratio between the actual pathway that a molecule travels through the pore space from one point to another in a porous media, to the straight pathway between two points as shown in figure 1 [6,7].

$$\tau = \frac{L_a}{L_s} \quad (1)$$

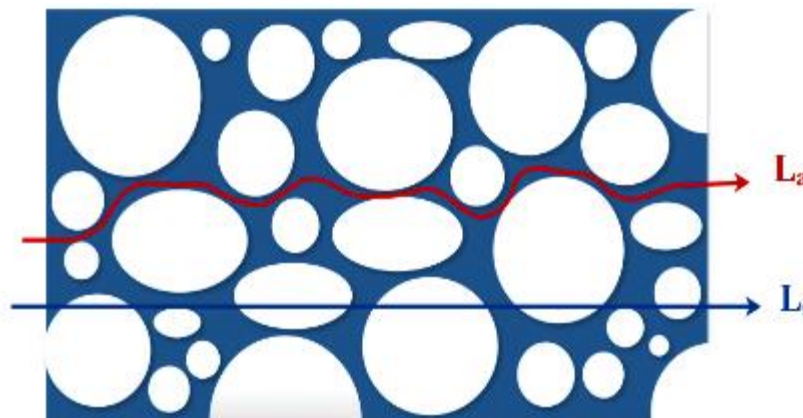


Figure 1. Microscopic cross section image of a porous medium showing both actual pathway and straight pathway traveled by a molecule.

As illustrated above, the value of tortuosity is always greater than one due to the higher tortuous pathway than the straight pathway as the tortuous path is affected by the pore space. Tortuosity considered one of the important parameter that contributes in many engineering and science applications. For example, separation of the mixture as it is simulated by models of fluids flow in tight rocks, water application as it is simulated by regional groundwater flow in a fractured aquifer, as well as, contaminant transport in fractured aquifer [8–12]. In addition, tortuosity is also important in studying soil properties and transport as it directly influences the transport processes of solute and gases into and across the soil. For example, it is used to the growth and the development of crop root [13–15]. In addition, it is one of the geometrical parameter that influence the transport of fluids in the soil as it is related to different characteristic parameters of porous media. For instance, tortuosity related to porosity, diffusivity, permeability, diffusion and gas transport parameters [16]. For instance, many studies have been numerically relating tortuosity to porosity [17].

Porosity is also considered one of the important parameter that controls fluid storage in aquifers, the extent and connectivity of the pore structure control fluid flow and transport through geological formations [18–20]. Where it is defined by the fraction of void volume over total volume as illustrated in figure 2 [21].

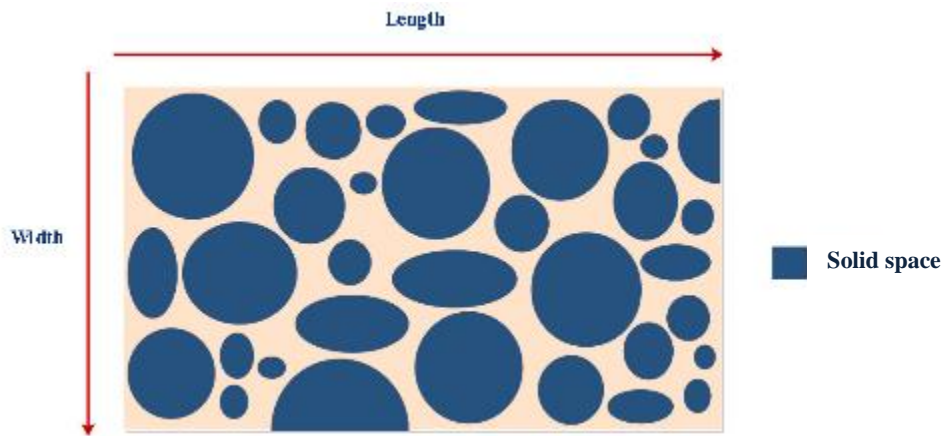


Figure 2. Microscopic cross section image of a porous medium showing solid space and void space.

Porosity and tortuosity are considered as a micro-scale parameter used in micro-scale equations in porous media such as nm and μm . However, most of the engineering application's scale is at the macro-scale system. Therefore, to validate applying micro-scale parameters at the macro-scale system, it is required to find the volume in which these properties are constant, which is the representative elementary volume (REV). Thus, volume-averaging method that governs the presence of representative elementary volume (REV) of the micro-scale parameters is essential. In other words, to upscale micro-scale parameters to macro-scale applications, it is important to prove the presences of REV of that property at a given spatial scale [22–24]. The concept of representative elementary volume (REV) relies on the knowledge of a continuum approach that deals with kinetic and mechanical analysis of materials modelled as a continuous mass rather than as individual particles. In other words, it deals with the macroscopic approach rather than a microscopic approach [25–27]. REV is the volume that each property of interest such as porosity, permeability, dispersivity and tortuosity, should be constant. To clarify more, all measured properties tend to decrease with increasing sample size. Thus, as the sample size increases, the variation in the measured

properties decreases which indicates the transition from a fluctuation property region which is a region that is dominant of microscopic inhomogeneity, into the REV region for any measured properties [28]. Figure 3 represents a conceptual schematic diagram that shows the idealized relationship between system property and sample volume measured (U). Generally, the relationship is interpreted into three different regions, initially at region 1 where spatial scales are small; the material property fluctuates rapidly since the material property is influenced by individual pores. Measurements constructed based on this scale will be considered as unreliable artefacts and are scale-dependent [29–31]. As the spatial scale increases, the material property tends to decrease and become uniformly independent as the measured scale increases. Where the geometrical property become a single-value in term of both time and location of that point, and this is because most of the pores factored into the average [30–33]. The volume means that the REV is the largest and can resist any volume changes throughout the entire volume [28]. The REV domain is defined as the range of volumes where the property of the material is single-value located between:

$$U_{min} \leq REV \leq U_{max} \quad (2)$$

In region 3, a further increase in the volume above U_{max} , the curve starts to increase slightly and this results in large field variability of macroscopic heterogeneity due to additional morphological structure [34]. Where the REV characteristic fades slightly resulted in an increase in the heterogeneity of the system as shown down below in figure 3.

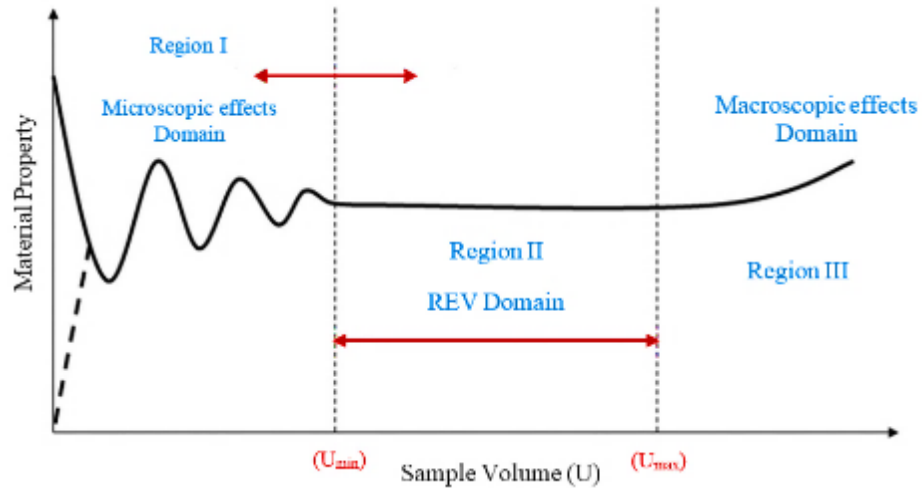


Figure 3. Schematic diagram of a change of a given material property over the change of volume.

This transition from a homogenous to a heterogeneous should be considered while determining the REV for a certain media. In other words, there are two main approaches commonly used to predict and study the behavior of materials such as macroscale or multiscale. Modelling based on the macroscale approach considers homogenous systems and this type of modelling is commonly used in hydrology literature and soil science. The other approach is multiscale-based where both micro and macro scale analysis is performed in which firstly at finite volume sizes, the microscale analysis is done; then, it will be incorporated into macroscale to give an evaluation of effective macroscale parameters [35–37]. In general, it was recognized that the characteristics of a porous media could affect size of REV. Moreover, each porous media has its own representative elementary volume (REV) for each parameter because REV varies from one physical property analyzed to another [38]. In addition, (Al-Raoush and Papadopoulos) [39] proved that the REV of any microscale parameter of concern should be determined based on their distributions over different volumes and should not be derived based on REV for other properties (e.g. porosity). Therefore, it is

important to find REV for any microscopic property including porosity and tortuosity and thus, relate them to some extent. This is because REV may differ from one property to another, therefore, the appropriate representative scale depends on which property is considered as well as system condition of interest [25,28,31,33,40].

REV determination is effective and essential for averaging, simulation and measurements because when the scale of measurements are representative and do compass the REV region, the resulted measurements will not show a variation that resulted with effective outcomes and accurately represent a larger system [41,42]. There are many applications based on REV concept such as contaminant migration modeling [43,44], application to the gas diffusion layer of PEM fuel cells [45], determining representative elementary volume for permeability in heterolithic deposits using numerical rock models [46], calculation of effective petrophysical properties in reservoir evaluation [47–49], and flow and reactive transport for CO₂ storage in carbonate reservoir [50–52]. The wide range of used applications based on the REV concept has been proved its important role in all hydrological and geophysical applications.

1.1 Objectives

The main objectives of this thesis is to relate representative elementary volume (REV) of tortuosity to that of porosity using computed tomography images. Moreover, to determine whether an REV for porosity is sufficient to define REV for tortuosity. These objectives were achieved through the following steps:

- 1- Used of Synchrotron-based X-ray microtomography high-resolution three-dimensional images for fifteen natural sand system developed by Al-Raoush [12].

- 2- Used two existing Matlab codes to find the porosity and tortuosity developed by Al-Raoush and Papadopoulos [39] and Al-Raoush [12] for each system.
- 3- Developed an efficient algorithm using Matlab to calculate REVmin of porosity and tortuosity.
- 4- Obtain REV analysis from the developed algorithm of porosity and tortuosity to observe and drive the relationship between them.

1.2 Thesis Organization

This report is organized as follows:

1. Literature review and background information about the studies that have been done in the representative elementary volume of both porosity and tortuosity field.
2. Methodology including data used, synchrotron micro-computed tomography, computation of tortuosity, and data analysis.
3. Deep description about the developed algorithm using Matlab to find REV of porosity and tortuosity.
4. Results and discussion that provide a comparison between them to drive the relationship between REV for porosity and REV for tortuosity.

CHAPTER 2: BACKGROUND AND LITERATURE REVIEW

Pore-scale physics and processes used to detect and study the performance of certain reservoir to accurately developed simulation framework that is accommodated at a pore-scale level for assessing unconventional oil and gas resources [53]. Moreover, aquifers that stored groundwater are considered one of the important component of freshwater resources [54,55], where the structure of these aquifers composed of granular porous media. Hence, it is very essential to study the structure and the compositions of the granular porous media, in order to investigate the macroscopic transportation of water and contaminant caused by groundwater overexploitation in the porous media [56–58]. The phenomena of macroscopic transportation of water and contaminant are related to the microscopic properties such as porosity, tortuosity, permeability, etc. Literature had spotted the light toward the relationships between the structures of porous media associated with their microscopic properties [59]. Therefore, to demonstrate this relationship and explore porous medium structure, many techniques have been widely used such as nuclear magnetic resonance. This technique applied magnetic field to the system and removed, causing disturbance of the equilibrium state of the system. Hence, different properties can be provided related to the pore-size distributions [60]. Moreover, in recent years, porous systems like natural rocks extracted from hydrocarbon reservoir had been studied via one of the useful technique, which is micro-scale x-ray computed tomography. This technique provides high-resolution 3D images of porous systems through which pore structure and its morphology can be characterized. Moreover, it can provide both statistical characterizations through different descriptors as well as used to solve mathematical differential equations [61]. Additionally, many recent publications have been proven the suitability of 3D imaging for investigating microscopic properties for different types

of rocks [62–64]. However, all the results will be implemented only at the micro-scale level in which these properties are introduced, whereas, it will not be representative at the macro-scale level in which the hydrological and engineering applications are executed. Therefore, several studies have been conducted to study property variation with different sample sizes in porous media at various scales defined as representative elementary volume, in order to verify that micro-scale properties are representative at macro-scale level [22,65].

2.1 Microscopic properties

Microscopic parameters are the geometrical properties that characterize the soil structure considering mainly porosity and tortuosity. Porosity is defined as the ratio of the volume occupied by the pores over the total volume [21]. Where the tortuosity is defined as the ratio of actual flow path length to the straight path length [66]. Both properties contribute to providing a full understanding of the mechanisms of the fluid flow as well as the complex structure of porous media. Moreover, many studies have been extensively investigated the transport in unconsolidated porous media that is influenced by the decrease of the volume due to the presence of solid particles where it is described by the porosity. In addition, the presence of solid particles increases the tortuous path where it is described by the tortuosity [10,67,68]. In literature, several approaches have been carried out to measure both porosity and tortuosity including analytical, experimental, and numerical simulations. As these properties are related to each other, many approaches were modelling the tortuosity as a function of porosity for fixed bed with identical packed particles [69,70]. Dealing with these properties at the macroscale is not valid as they are adapted at microscale level, unless they are representative, which mean they fall

under the range of representative elementary volume (REV). REV is defined as the volume at which the microscopic property variation is stable at the macroscopic scale. Several researchers have been conducted the REV analysis to develop a model that describe one or more microscopic properties [71–74]. For example, Ahmadi et al. [74] proposed an analytical model of tortuosity and permeability established within a representative elementary volume (REV). Moreover, Freytag and Roque [73] represented an analytical model relating the porosity and the tortuosity of polyhedral grains size based on the representative elementary volume (REV) model. Recent advances technologies have been increasingly using computed tomography to obtain three-dimensional images for determining tortuosity of certain porous media [75–78]; for the development of algorithms that will aid to visualize non-destructively the interior of porous media [78–80]. Al-Raoush and Madhoun [81] had developed an efficient, accurate and accessible algorithm implemented as Matlab code to determine tortuosity of unconsolidated porous media from three-dimensional computed tomography images. This code is sufficient as it can effectively find all connected continued paths at a very short time. Moreover, three-dimensional images of different sand systems were used for the validation of their algorithm. The main outcome of this study is that the developed algorithm code was successfully computed the tortuosity values for any unconsolidated porous system regardless the geometry of particles. Therefore, this code can be generalized to calculate tortuosity for all unconsolidated porous system.

2.2 Representative elementary volume (REV)

Representative elementary volume is defined as the smallest volume in which the microscopic property become representative of the system at the macroscopic scale. Where it is used for modelling the transport properties of macro-scale porous

media [82]. In literature, studies related to REV may vary in term of the type of investigated rock such as real sample rocks or numerical rock models, microscopic property, sample size and type of measuring techniques. Vik et al. [28] investigated the existence of REV of various properties at different sample size focus on the investigation of real rock. All measured properties of the vuggy carbonate material decreases in variability, while increasing the sample size. This was done by measuring the properties at a large volume and afterwards, each sample volume is divided into two equal sub volumes, in which continuously the property is measured. However, a certain amount of material can be lost during the cutting procedure, and this may cause some differences between the preformed physical characterizations of each split at different scales. Moreover, Jackson et al. [83,84] used three-dimensional models to characterized the reservoir properties including connectivity and permeability of real sample rock blocks. The size of the models used was smaller than typical grid block and larger than the core plug. The main result was found is that at the scale of the reservoir model, the size of the core plug sample size was not representative. Therefore, it was difficult to capture the connectivity as it is highly dependent on length scale occupied. Thus, it is important to consider the accurate average scale of measurements. Other researchers accredited to find the appropriate average scale size that is relative to the scale of the heterogeneities [85,86]. The choice of element size related to the representation is critical, where the analysis of representative size could be conducted over different sizes of interest such as length, area and volume (REL, REA and REV) as well as it can be determined for different type of porous media, parameters and measurements scales. The use of sample associated with representative size is highly recommended since any property will be no longer dependent on the size. In

other words, dealing with a sample size that is not a representative size might be highly dependent on the spatial structure. Thus, analyzing a representative sample give an indication of the soil quality and quantity of measurements such as a sample with REV [34]. REA was first initiated by Wood et al. [87] that spread the idea of a representative scale at which the spatial behavior remains stable without showing variation. There are various applications have been built under the idea of REA including soil hydrology and soil pores observations [88,89]. In a more recent publication of the REA concept, Borges and Pires [90] found 4% reliable results of REA of density measurements for the soil of clay texture with samples volume ranging from 50 to 100 cm³ and this was enough to produce representative density results. In addition, using gamma-ray computed tomography, which is considered to be one of the excellent techniques that provide both qualitative and quantitative measurements without changing the physical structure of the sample, has proven to be satisfactory.

Another area that has been intensely developed in the recent years is the use of numerical simulations; recent studies have dealt with the estimation of REV of porous media using numerical methods that are based on computational techniques such as finite element method (FEM) and discrete element method (DEM). These approaches are strongly dependent on the microstructure and the macrostructure mechanical behavior of the cohesive granular porous media. For instance, DEM method used to model and study the microstructure of granular porous media whereas, FEM method used to analyze at a large scale, which is macrostructure scale [91,92]. A discrete element method was applied to determine the representative elementary volume (REV) for three-dimensional polydisperse granular sphere where both geometrical and mechanical REV's parameters were

estimated. Findings revealed that for sphere packing both the geometrical and mechanical REV were found to be different in sizes. Moreover, the REV for these parameters is not affected by the heterogeneity of the system [11]. Additionally, there are several numerical techniques that were implemented to study and analyze the representative elementary volume of porous media for different properties mainly about porosity, specific surface area, permeability and tortuosity, to find relationships between them. Mostaghimi et al. [11] simulated finite difference method to analyze permeability for consolidated and unconsolidated porous media using a set of computed tomography images at micrometer resolution. The main outcome of this paper was that the REV for permeability is larger than REV for static properties such as porosity, and this is because REV for permeability account for the tortuous paths resulted in larger REV than static parameters e.g. porosity.

Many recent advance studies have been applying micro-computed tomography techniques for establishing soil properties for different hydrological applications [30,39,93,94]. The main advantage of micro-computed tomography is that it provides three-dimensional imaging in a non-destructive way. X-ray micro-computed tomography is widely used technique of providing cross-sectional views depending on the amount of x-ray absorbed. Hounsfield [95] was pioneered to promote computed transverse axial scanning images. After that, many commercial applications have been developed using high voltage x-ray computed tomography, used to investigate the internal structure of different objects especially in geoscience applications. This non-destructive technique provides high resolutions of 3D images at a hundred nanometers level of internal structural. However, it is limited by some operational issues related to the 3D analysis from the reconstructed data. For instants, due to the presence of wide variety of different sample size, composition

and shape this will require multiple of computed tomography setups, which will eventually yield different results [90,96]. Accordingly as an alternative and enhanced source than x-rays is Synchrotron radiation combined with x-ray because they provide very intense, naturally collimated, narrow bandwidth and tunable photon beams [29]. Where many researchers intensively used Synchrotron x-ray radiation technique to generate, computed tomography images to determine REV of different microscopic parameters as well as various soil properties. For instance, Al-Raoush et al. [97] investigated the pore network structure using high-resolution 3D images constructed using Synchrotron x-ray computed tomography. In addition, they were able to calculate REV as well as some geometrical properties such as porosity and specific surface area. Moreover, Culligan et al. [98] used a synchrotron-based computed tomography technique to obtain air-water interfaces images of repacked sand and glass beads system at approximately 12 μ m resolution. Moreover, Pot et al. [99] studied the distribution of water and air in soil samples constituted of repacked aggregates via Synchrotron X-ray computed tomography at a resolution of 4.6 μ m. More advanced research by Andrew et al. [96] was able to measure the contact angle of CO₂-brine interfaces onto the solid surface of limestone at a resolution of 2 μ m. Besides that, studying the REV of porosity, tortuosity and connectivity are important as they are related to soil water management, where it provides sustainable and efficient agricultural production. For instance, recently Borges et al. [100] used 3D micro-computed tomography technique to obtain images to investigate REV for different soil properties specifically including tortuosity. The resulted showed variation for small investigated subvolumes which is standard, reaching REV of tortuosity around 10,841 mm³. Other researchers have discussed the same kind of finding relevant

soil properties [101–103]. Furthermore, x-ray computed tomography technique has proved by many researchers its efficiency to analyze different microscopic soil properties such as porosity, connectivity, permeability, particle distribution and tortuosity [104–106]. For example, many studies investigated REV for individual macroscopic properties such as porosity, permeability, tortuosity, and specific surface area. For instance, de Araújo et al. [107] investigated the existence of REV for porosity and permeability of the limestone sample using computed tomography images. The results showed REV length was found to be around 15×10 mm for the REV length and thickness respectively and 100 slices of height, by that all the results were relevant showing the homogeneity of limestone. The drawback of this study is that using limestone that verified its homogeneity visually is not convenient as from the structure it can be observed. Recent studies had determined REV size based on combining two parameters. Shah et al. [108] determined the REV for two microphysical parameters, which are porosity and permeability using micro-computed tomography imaging technique and Lattice Boltzmann (LB) simulations. The main result of this study is that the required volume needed to determine the representative system size is small, as the two parameters started to decrease rapidly as the volume increases. However, the LB technique required high computational time for single-phase system, therefore, it is not accurate for the multiphase system [109–111]. Moreover, Mostaghimi et al. [112] used computed tomography technique to relate the REV for porosity and REV for permeability for sandstone and carbonate samples. The results show a permeability variation for $300 \times 300 \times 300$ voxels is continued while reaching the REV for porosity around 2mm. In other words, it was found that the REV for permeability $> 2mm$ higher than for porosity, as it should account for the tortuosity and connectivity of the pores. In a comparative

study, Zhang et al. [31] used lattice Boltzmann simulations on pore geometries reconstructed from computed microtomography images to find REV of porosity and permeability. They found the linear dimensions which is the REV is reached for porosity and permeability is around 1.71 mm and 2.57 mm respectively. Where it is larger than Mostaghimi et al. [112] found. In contrast, other studies including [113] attempt to use the REV sample two-dimensional, representative elementary volume (REV) of circular particles, to calculate tortuosity and developed a model that relates tortuosity to porosity. Although the developed model agrees well with the assumptions and their experimental values, it could not be generalized as it is limited to 2-dimensional systems only with ideal geometry e.g. spherical particles. Same idea was implemented by various researchers [73,74,114,115]. For instance, Freytag and Roque [73] represented an analytical model relating the porosity and the tortuosity of polyhedral grains size based on the representative elementary volume (REV) model. Furthermore, they explore the influence of packing parameter B that directly affected the porosity and the tortuosity of a granular porous media. Their results showed that different packing parameter B which is ranged from 0 to 1, influenced different grain size. Moreover, this approach is only valid for the medium has elementary volume homogeneous in porosity and tortuosity.

Another technique that has been widely used in many studies within this field is light transmission technique [43,108,116–118]. For example Wu et al.[43,118] developed long-term migration experiment using dense non-aqueous phase liquids (DNAPLs) to perform two-dimensional (2D) sandbox in which porosity and various system variables were precisely specified by light transmission techniques over the whole migration process. Moreover, they proved their argument regarding their

choice of light transmission technique by claiming that advanced technologies that use Synchrotron x-ray and gamma-ray microtomography as a source of radiations are restricted by some hazardous environmental limitations, high-energy requirements and cost issues regarding complex equipment implementation. Continuation research verified the experimental work that was done by Wu et al. [43,118] was developed by Wu et al. [119] to simulate the DNAPL in heterogeneous translucent porous media based on REV estimations. Then, this model was improved to a 3D model for spherical solid particles and the model showed satisfactory results compared to the experimental data of tortuosity Wu et al. [120]. The main finding is that REV for porosity is always lower than for tortuosity, thus, the emphasis that REV should be determined for each property as well as excluding the idea of relating or finding a relationship between the two REV properties. Although, this model agrees well with their experimental data; however, this is not realistic because it is only applicable for spherically shaped particles not accounting for irregular shapes.

Hence, knowing the significance of finding a relationship between REV for tortuosity and porosity and its impact on many engineering applications. There is a need to determine whether an REV for porosity is sufficient to define REV for tortuosity for different types of porous media independent on the geometry of particles, which is realistic and could be generalized in a real reservoir. Thus, here comes the novelty of our research were we aim to use a 3D model that was developed by [39] and [12] to determine the REV for tortuosity. Different systems with a different range of grain sizes and shapes were analyzed with high-resolution three-dimensional images using synchrotron-based X-ray microtomography with the purpose of finding REV of porosity and tortuosity. Then, to observe whether

the REV for tortuosity is sufficient to be defined by the REV of porosity.

CHAPTER 3: METHODOLOGY

3.1 Data

Data have been obtained from experiments conducted by Al-Raoush, 2014 [12] will be used to developed 3D computed tomography images using synchrotron x-ray computed tomography. Different sand samples with different physical characteristics were used to model the porous media structure where the physical properties are given in table 1. Silica and quartz are the two different shapes of sand particles that account for rounded geometry and angular geometry respectively. Moreover, mixed sand of both silica and quartz was created by mixing equal masses of both types of sands. The samples were packed in different systems where each system specified with different ranges of particle diameter and geometry such as *systems (1-6)* were assigned with silica geometry, *systems (7-12)* were assigned with quartz geometry, and *systems (13-15)* were assigned with a mixture of both type silica and quartz. Cross-sectional views of each type of porous media as well as 3D images of the cross-sections were illustrated in figure 4.

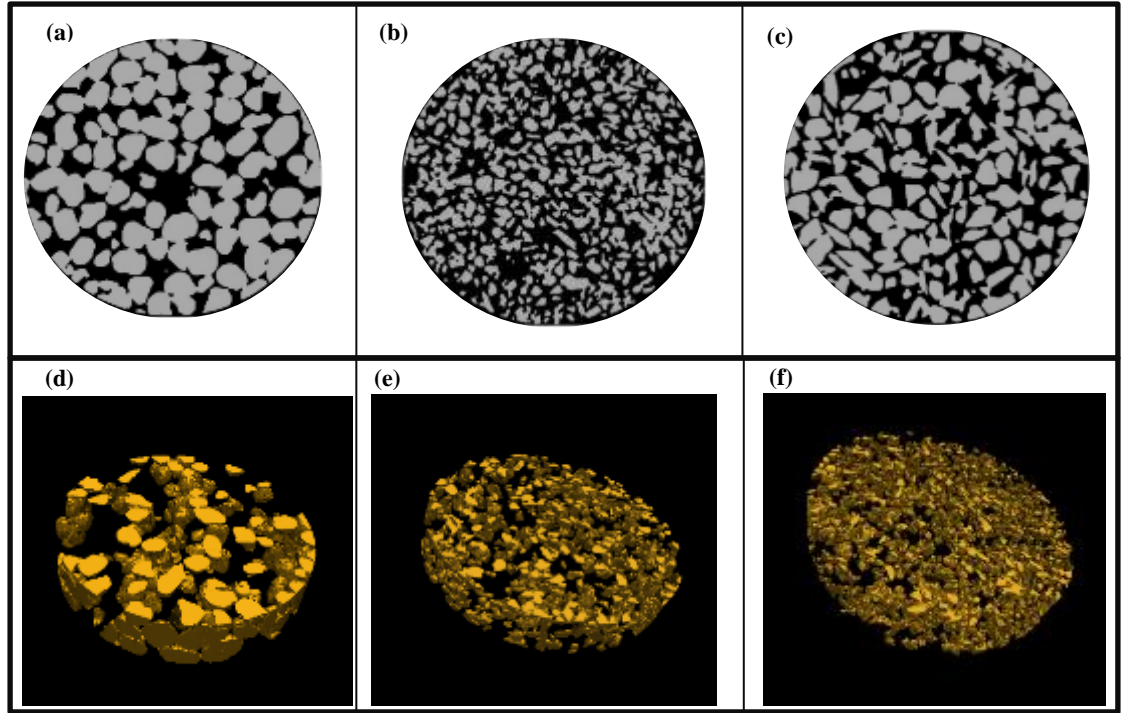


Figure 4. (a) Cross-sectional image of system 1 with silica particles geometry, (b) Cross-sectional image of system 7 with quartz particles geometry, (c) Cross-sectional image of system 13 with silica and quartz mixed particles geometry, (d) 3D image of system 1 with silica particles geometry, (e) 3D image of system 7 with quartz particles geometry, and (f) 3D image of system 13 with silica and quartz mixed particles geometry.

Each system has particle size ranged between (30-100) μm . In addition, D_{50} , which is the median grain diameter, for silica geometry ranged from 0.433 mm to 0.195 mm, for quartz geometry, ranged from 0.316 mm to 0.178 mm and for the mixed of both silica and quartz is ranged from 0.298 mm to 0.185 mm. The sphericity index, Ψ , was determined for each column as it describes how closely the shape of a grain approaches a sphere shape. It is calculated via the following equation [12].

$$\Psi = \frac{SA_n}{SA_p} \quad (3)$$

Where SA_n is the nominal surface area and SA_p is the surface area of the grain, the

sphericity index ranges from 0-1, where the maximum value of 1 indicates perfect sphere.

The roundness index, X_v , describes how closely the shape of the grain approaches perfect circle. In other words, describes the curvature of a grain's corner. It is computed using the following equation [12]:

$$X_v = \frac{3V_p}{DS A_p} \quad (4)$$

Where D is the diameter of a minimum sphere circumscribing a gravel particle and V_p is the volume of a gravel particle. The sphericity index, Ψ , for silica sand geometry ranged from 0.852 to 0.890. Whereas, for quartz sand geometry ranged from 0.792 to 0.815. It is observed that the sphericity index for the silica sand geometry is higher, that quartz geometry as silica grain resembles a sphere shape. The same conclusion could be driven for the roundness index, as it ranged for silica geometry from 0.798 to 0.840 and for quartz geometry ranged from 0.717 to 0.744. Moreover, the porosity values for silica sand geometry ranged from 0.323 to 0.380 and for both mixed and quartz sand geometry ranged from 0.393 to 0.489. The higher ranged of porosity values for both mixed and quartz sand geometry is due to the difficulty of obtaining pores space in systems composed of non-spherical grains. All values of mesh size distribution, D_{50} , porosity, sphericity index, and roundness index are reported in table 1.

Table 1. Physical Properties of the Porous Media Including Porosity, Mesh Size Distribution, D_{50} , Sphericity, and Roundness [12].

Geometry	System #	Porosity (Φ)	Mesh Size (mm)	D_{50} (mm)	Sphericity	Roundness
Silica	1	0.327	d1: (30-40)	0.433	0.89	0.84
	2	0.369	d2: (40-50)	0.352	0.864	0.82
	3	0.356	d3: (50-60)	0.267	0.849	0.801
	4	0.382	d4: (60-100)	0.196	0.852	0.798
	5	0.33	d5:10% d1+30% d2+50% d3+10% d4	0.271	0.852	0.805
	6	0.323	d6:5% d1+50% d2+30% d3+15% d4	0.258	0.857	0.808
Quartz	7	0.47	d1: (30-40)	0.316	0.792	0.717
	8	0.462	d2: (40-50)	0.276	0.794	0.723
	9	0.488	d3: (50-60)	0.237	0.801	0.738
	10	0.505	d4: (60-100)	0.178	0.815	0.744
	11	0.455	d5:10% d1+30% d2+50% d3+10% d4	0.233	0.81	0.74
	12	0.489	d6:5% d1+50% d2+30% d3+15% d4	0.213	0.809	0.739
Mixed (Silica & Quartz)	13	0.398	d7: 50% d2 (silica) +50% d2 (quartz)	0.298	0.819	0.754
	14	0.408	d8: 50% d3 (silica) +50% d3 (quartz)	0.252	0.822	0.765
	15	0.393	d9: 50% d4 (silica) +50% d4 (quartz)	0.23	0.831	0.771

3.2 Synchrotron micro-computed tomography

Synchrotron micro-computed tomography is an advanced technology provides a high intensity with high flux source of x-ray beam to visualize the structure of porous media. The imaging stage was done by the GeoSoilEnviroCARS 13-BM-D beamline at the Advanced Photon Source, Argonne National Laboratory, and Illinois. Image reconstruction algorithms [12], this technique converts the x-ray beam data into cross-sections to obtain three-dimensional images. The samples were compacted in columns and scans with different energies including 33.269 keV, 33.069 keV and 36.085 keV, where it was obtained at mid portions of the columns using x-ray beam. Then, the cross-sectional images (slices) is constructed via using indicators that recorded the x-ray beam that passes through a section of the sample. After that, the computer receives all the registered image data to convert them into a series of 2D multiple cross-sectional images. A series of 2D projections are gathered to generate 3D images. The size of the image used was $696 \times 696 \times 520$ voxels and the image resolution was $9.6 \mu\text{m}/\text{pixel}$ in all directions [12].

3.3 Computation of tortuosity

Tortuosity was computed using Tort3D code, a MatLab code developed by Al-Raoush and Madhoun [81] used to compute the geometric tortuosity from 3D images of unconsolidated porous media. Tort3D code measures geometric tortuosity from 3D images of porous media. In addition, random paths codes where it is optimized to find out from binary image all possible tortuous paths in a porous media system. More details of code can be find in Al-Raoush and Madhoun [81], a brief description is given below.

As the main idea of this code is that it reads all connected paths in the segmented

image in order to utilize the medial surface of the void space, to finds all possible tortuous paths required to compute tortuosity. By this approach, it limits the time and memory requirements for input parameters and user Interaction. Hence, the code is user-friendly and easy to use, compute the connectivity and tortuosity in x, y and z-direction. The code computes tortuosity as:

$$Tortuosity (\tau) = \frac{\text{Average of all path lengths}}{\text{Size of the image in the direction of flow}} \quad (5)$$

In this analysis, this code was executed to find the tortuosity values for all the systems as shown below in table 2. It is observable that the tortuosity values for silica sand geometry are ranged from 1.39-1.50, which is lower than mixed sand and quartz sand geometry ranging from 1.51-1.97. In addition, this is due to longer pathway of obtaining dense compactions systems composed of non-irregular grains.

Table 2. Porosity and Tortuosity Values of all systems.

Geometry	System #	Porosity (Φ)	Tortuosity (τ)
Silica	1	0.327	1.497
	2	0.369	1.488
	3	0.356	1.467
	4	0.382	1.392
	5	0.33	1.419
	6	0.323	1.485
Quartz	7	0.47	1.967
	8	0.462	1.652
	9	0.488	1.640
	10	0.505	1.527
	11	0.455	1.732
	12	0.489	1.774
Mixed (Silica & Quartz)	13	0.398	1.574
	14	0.408	1.606
	15	0.393	1.634

3.4 Calculation of representative elementary volume (REV)

For the REV analysis, twenty sub-volumes were selected inside the total volume ($696 \times 696 \times 520$ voxels) for each column. Considering the shape of the 3D image is cylinder with x, y, and z coordinates where z-axes represent the height of the cylinder and r is the radius of the cylinder base. The sub-volume selection was made according to two schemes:

1. Changing the radius while fixing the height.
2. Changing both height and radius.

Height varies from 520 to 120 voxels (4.99-1.15) mm and the radius ranges from 275

to 75 voxels (2.64-0.75) mm. The total volume of each sub-volume is calculated simply using:

$$V_{cylinder} = \pi r^2 H \quad (6)$$

With sizes varying from 1.87 to 109.26 mm³ as shown in Table 3 where all the subvolumes were occupied for REV analysis, were summarized as well as for 3D schematic diagram represented in figure 5 visualize how the subvolumes are selected.

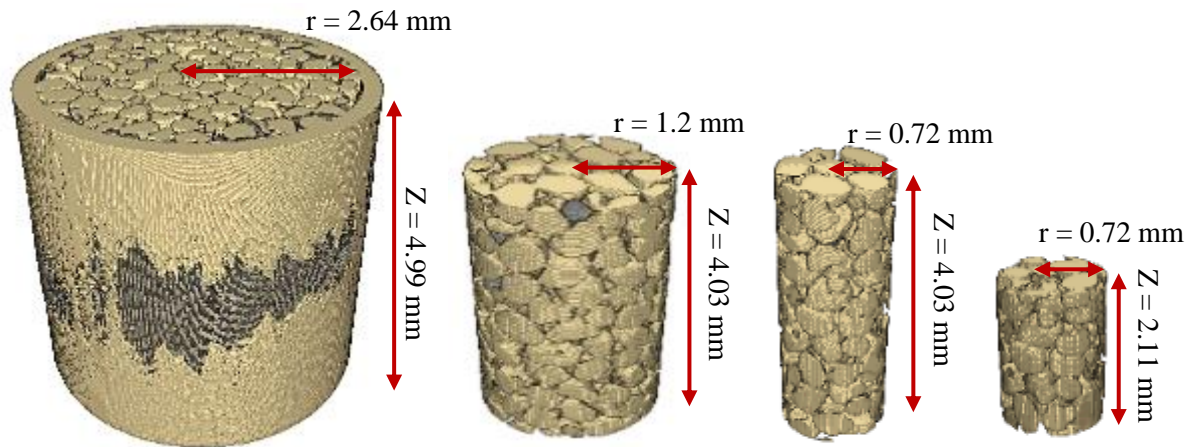


Figure 5. 3D images showing the subvolume selected for REV analysis.

Table 3. Sub-Volumes Selected Inside The 3D Micro-Computed Tomography Images for REV Analysis.

Image	x (mm)	y (mm)	z Height (mm)	radius (mm)	Volume (mm ³)
1	6.68	6.68	4.99	2.64	109.26
2	6.68	6.68	4.03	2.64	88.24
3	6.68	6.68	3.07	2.64	67.22
4	6.68	6.68	4.03	2.16	59.07
5	6.68	6.68	2.11	2.64	46.20
6	6.68	6.68	3.07	2.16	45.00
7	6.68	6.68	4.03	1.68	35.73
8	6.68	6.68	2.11	2.16	30.93
9	6.68	6.68	3.07	1.68	27.22
10	6.68	6.68	2.11	1.68	18.71
11	6.68	6.68	4.03	1.2	18.23
12	6.68	6.68	1.15	2.16	16.86
13	6.68	6.68	3.07	1.2	13.89
14	6.68	6.68	1.15	1.68	10.20
15	6.68	6.68	2.11	1.2	9.55
16	6.68	6.68	4.03	0.72	6.56
17	6.68	6.68	1.15	1.2	5.20
18	6.68	6.68	3.07	0.72	5.00
19	6.68	6.68	2.11	0.72	3.44
20	6.68	6.68	1.15	0.72	1.87

3.5 Data Analysis

3.5.1 Constructing distributions curves of porosity and tortuosity

For each column, porosity and tortuosity were computed for each sub-volume selected inside the whole volume using Tort3D [81]. The code reads segmented images and finds all possible tortuous paths required to compute tortuosity. It operates a guided search for connected paths in the void space of the image utilizing the medial surface of the void space. Moreover, porosity was calculated via MatLab utilizing the idea of

finding the void space over the total volume of the sample. Figures (6-8), shows the distribution curve of tortuosity and porosity over different volume in (mm) for system_1, system_7, and system_15. The other distributions curves are in Appendix B.

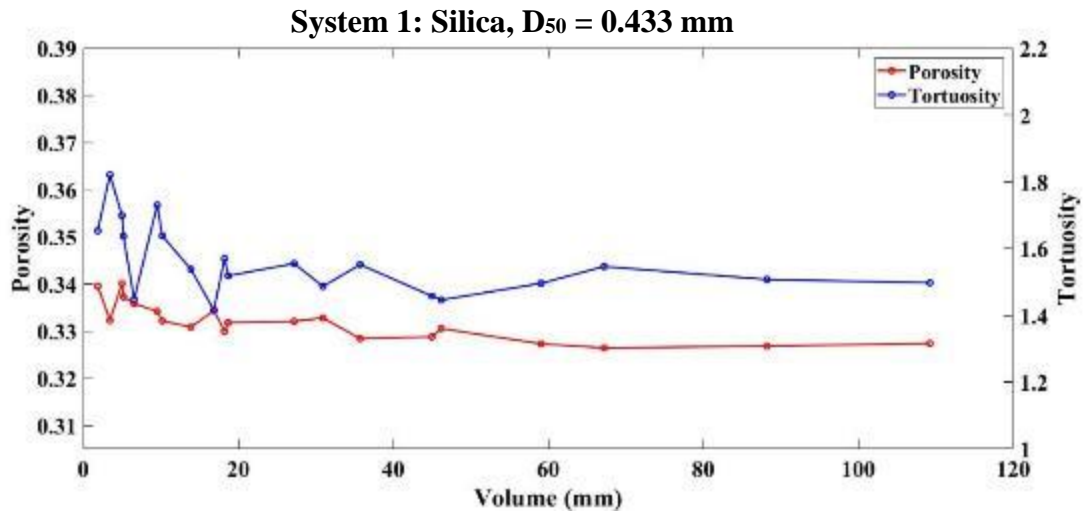


Figure 6. Porosity and tortuosity distribution curve of system 1.

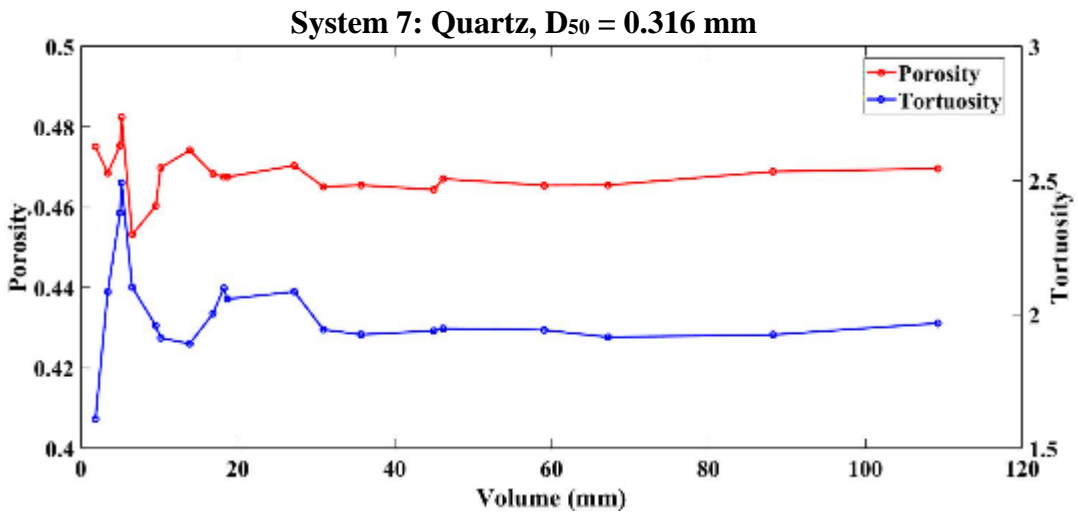


Figure 7. Porosity and tortuosity distribution curve of system 7.

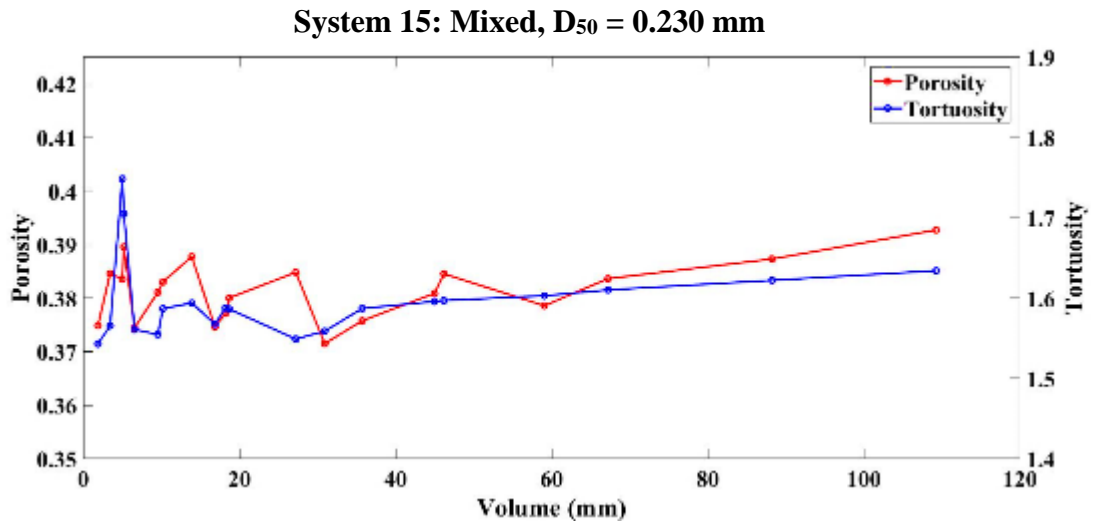


Figure 8. Porosity and tortuosity distribution curve of system 15.

3.5.2 Computing REV_{min} for porosity and tortuosity

To compare between the two properties it was required to find the representative elementary volume (REV) of each property. Therefore, a MatLab code was executed utilizing the idea of finding the slope of the distribution line between two points and compared by a specific tolerance. To clarify more the following steps will explain the steps that were used to calculate the REV of porosity and tortuosity:

- 1- The volume values were loaded for each sub-volumes in the system as well as the porosity and tortuosity values.
- 2- The slope between each two point was found. For instance, the difference between two points of the porosity were divided by the difference of the volume at these points (slope = $\frac{P_2 - P_1}{V_2 - V_1}$).
- 3- Then, this slope was compared to a very small value approximately zero in order to find the region where the distribution line become constant and almost horizontal line.
- 4- All the values that satisfied the condition, which are the values that were less than the tolerance will be saved in matrix called (i.e. REV_p for porosity)

- 5- In most cases, some values can behave stagnant at the beginning under the microscopic effects then fluctuates as shown in Figure 10. Thus, to account for continuous smooth stagnant REV region, the size of REV_p matrix was determined.
- 6- Then, for loop was generated for this matrix (REV_p), hence to find the difference between the sizes of the matrix and choose that is continuous (e.g. if the size of REV_p matrix is [2,4,5,7,8,9] the value that will be resulted from the for loop = 7]. In order to guarantee continuous follow of smooth horizontal line where the difference must be equal 1.
- 7- Finally, the value of REV will be assigned to the volume correspond to the first value that satisfied the previous condition (e.g. REV_{min} = volume (REV_p (7))).

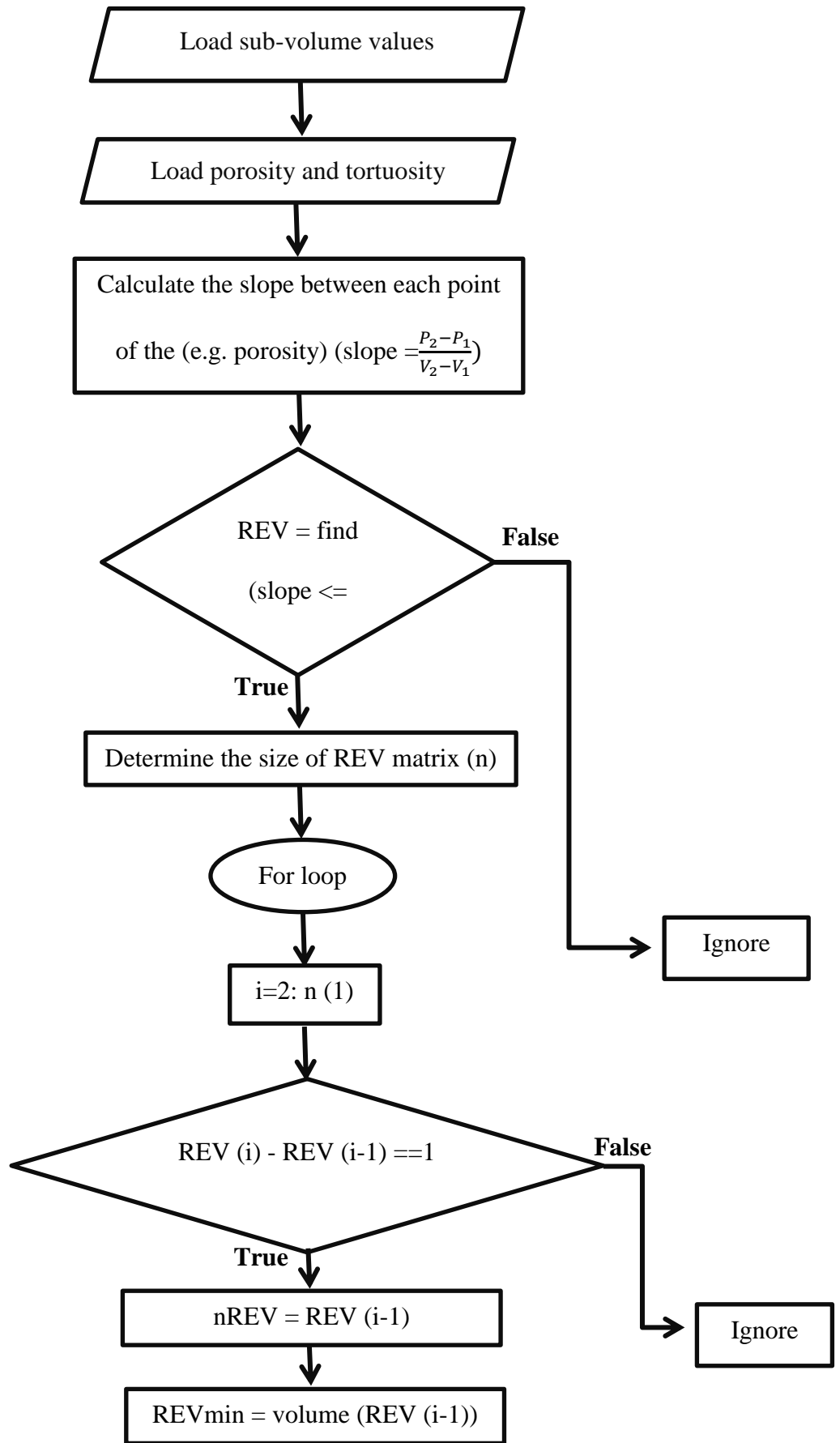


Figure 9. Flow chart of REVmin code.

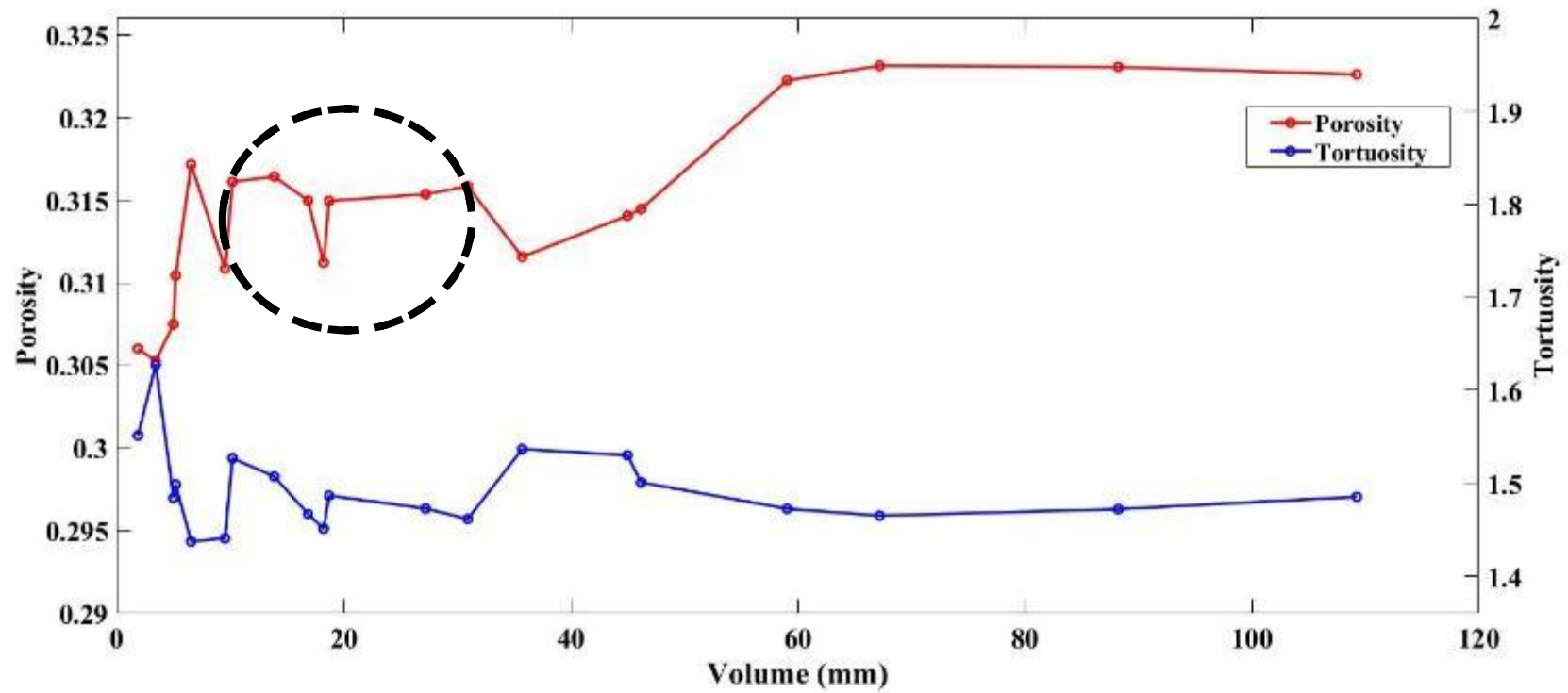


Figure 10. Using the distribution curve of system_5 as an example to clarify the idea of continuous smooth REV region.

CHAPTER 4: RESULTS AND DISCUSSION

The results found via running the developed code to compute REVmin for porosity and tortuosity are presented in distributions curve as shown below in Figure (11-25):

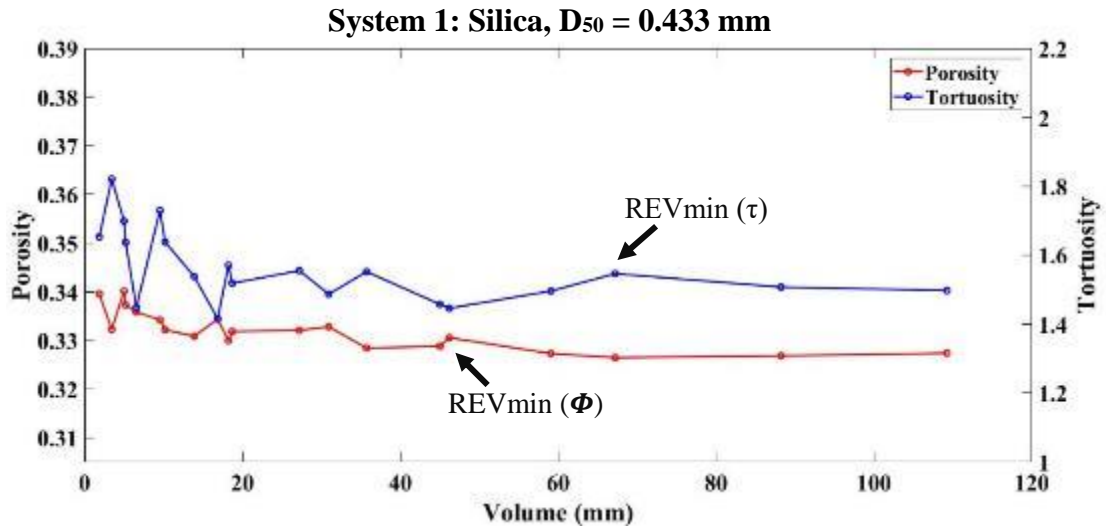


Figure 11. Distribution curve of porosity and tortuosity for system 1 marked with the REVmin values of both properties.

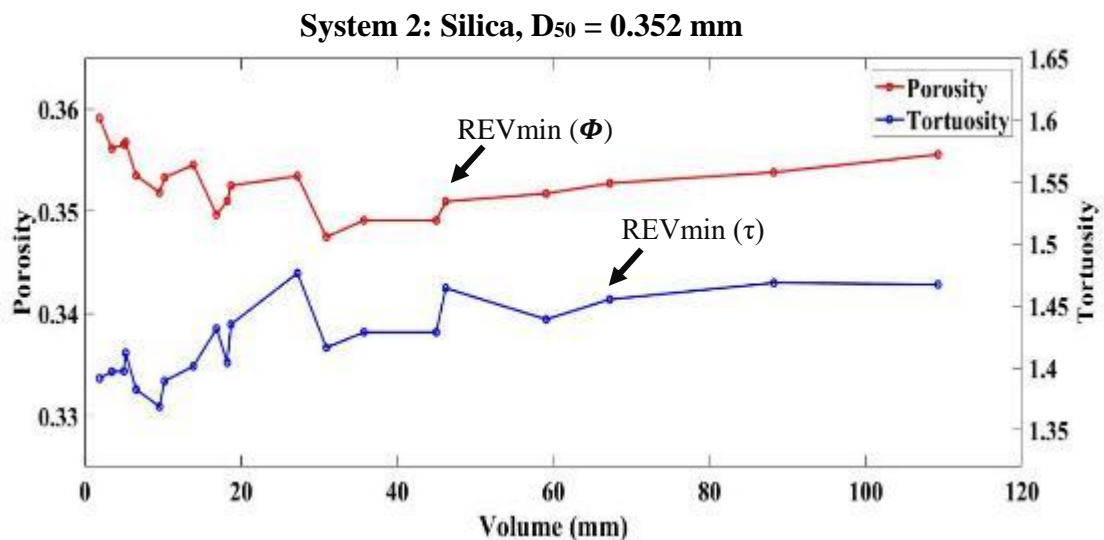


Figure 12. Distribution curve of porosity and tortuosity for system 2 marked with the REVmin values of both properties.

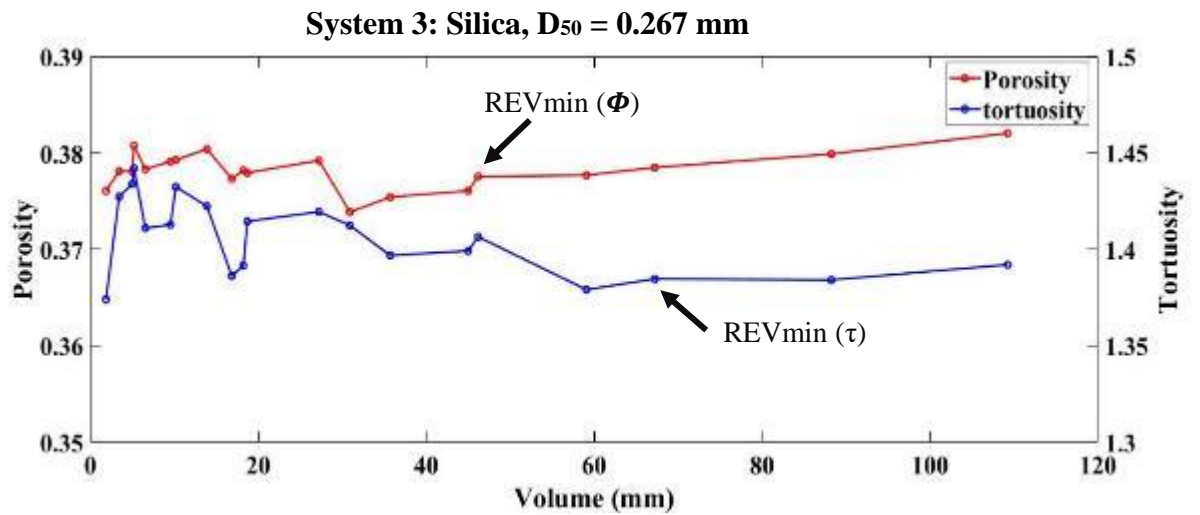


Figure 13. Distribution curve of porosity and tortuosity for system 3 marked with the REVmin values of both properties.

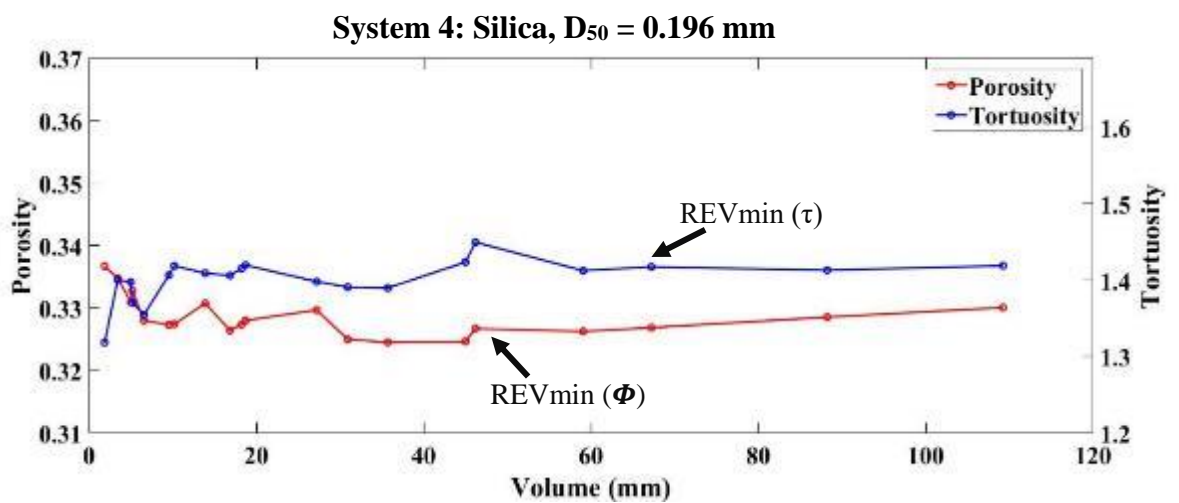


Figure 14. Distribution curve of porosity and tortuosity for system 4 marked with the REVmin values of both properties.

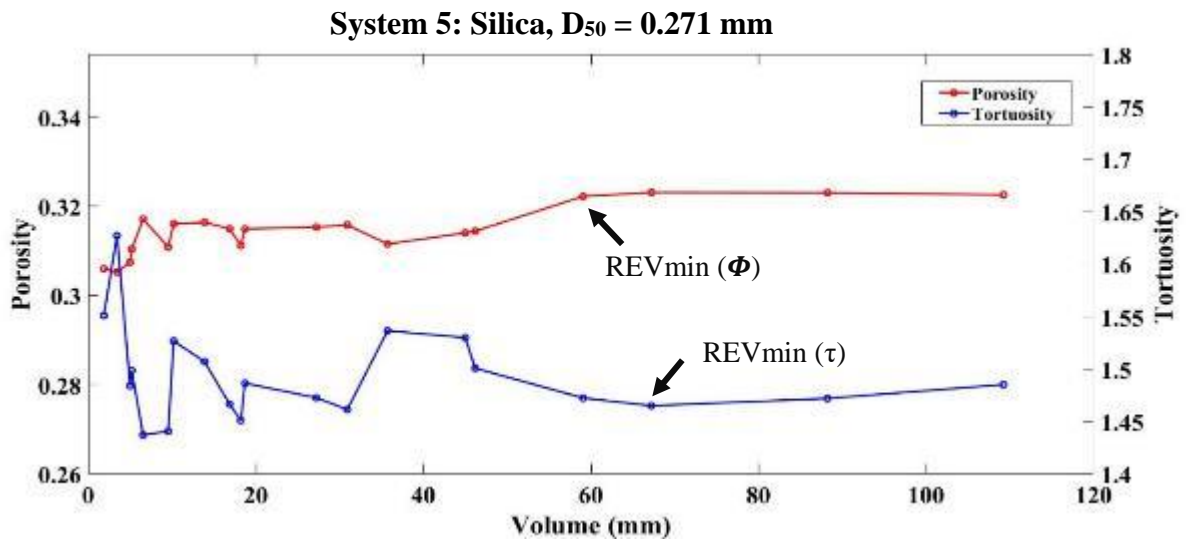


Figure 15. Distribution curve of porosity and tortuosity for system 5 marked with the REVmin values of both properties.

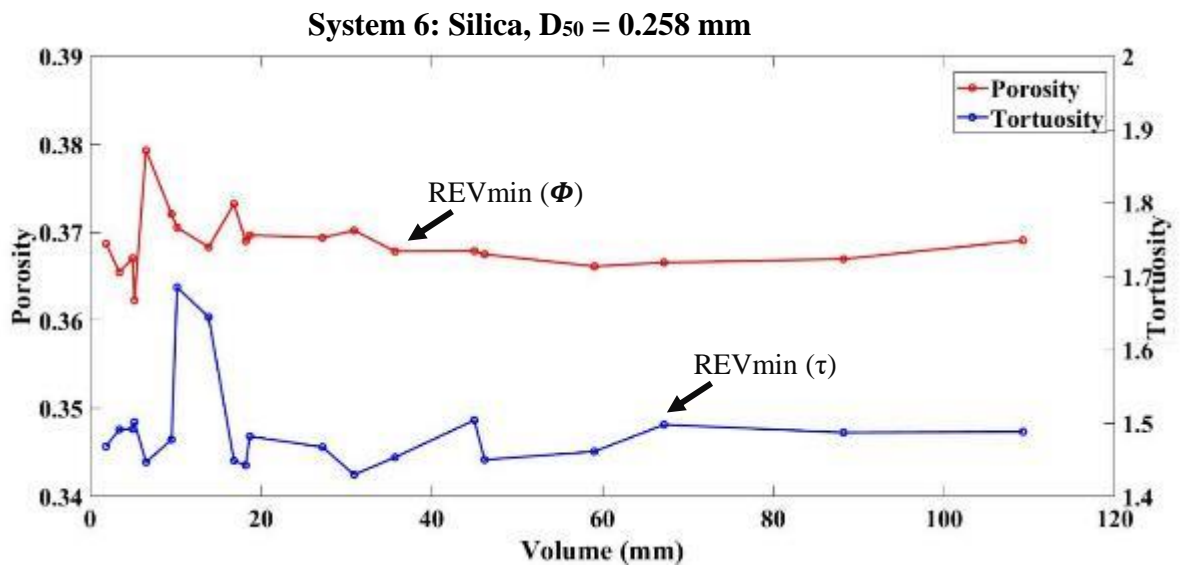


Figure 16. Distribution curve of porosity and tortuosity for system 6 marked with the REVmin values of both properties.

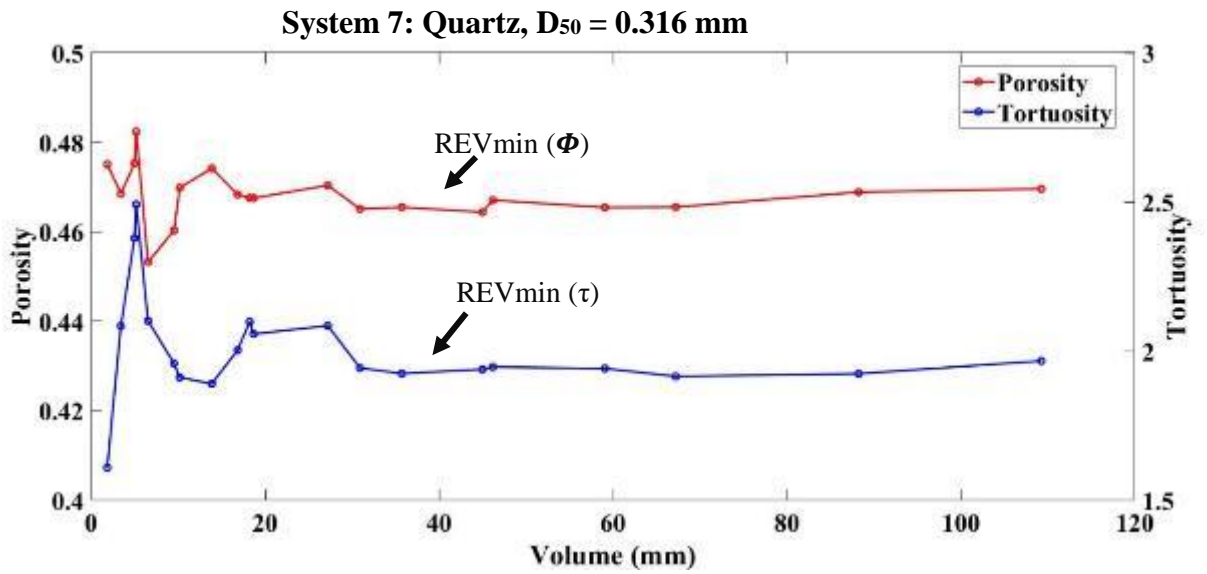


Figure 17. Distribution curve of porosity and tortuosity for system 7 marked with the REVmin values of both properties.

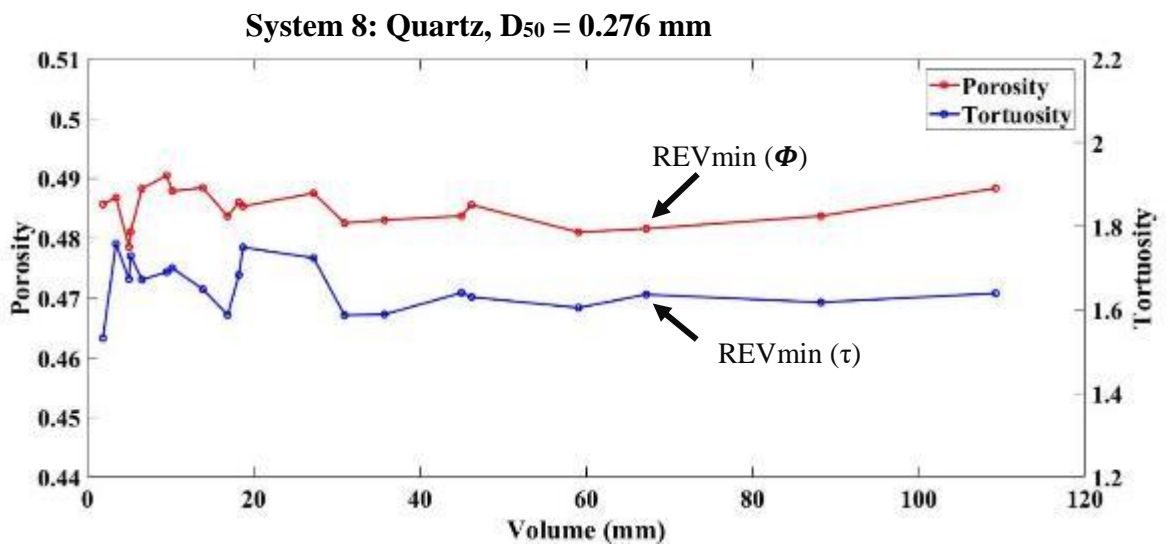


Figure 18. Distribution curve of porosity and tortuosity for system 8 marked with the REVmin values of both properties.

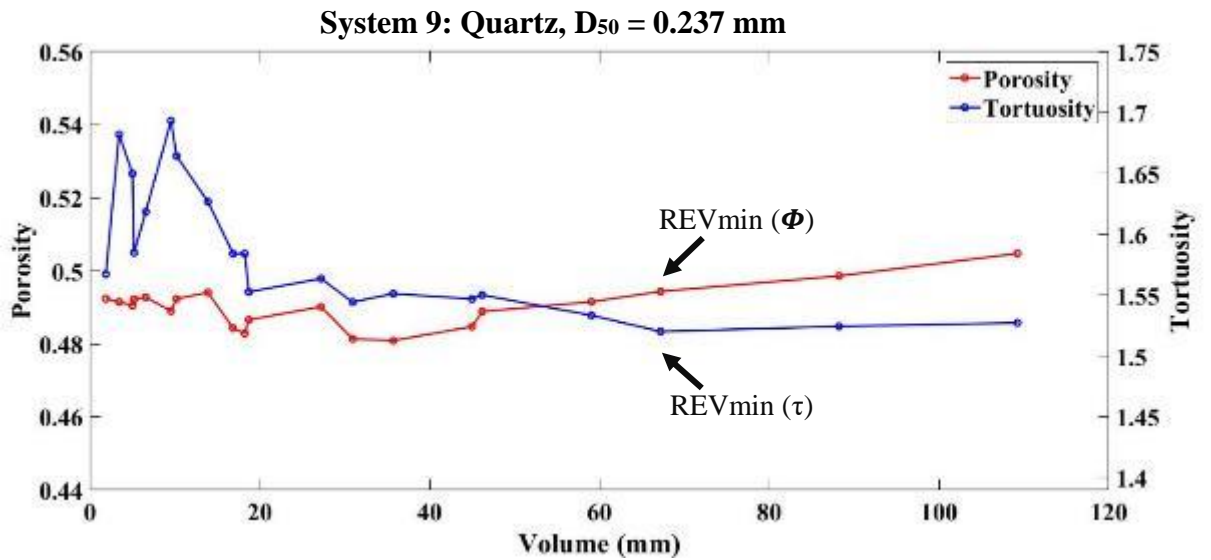


Figure 19. Distribution curve of porosity and tortuosity for system 9 marked with the REVmin values of both properties.

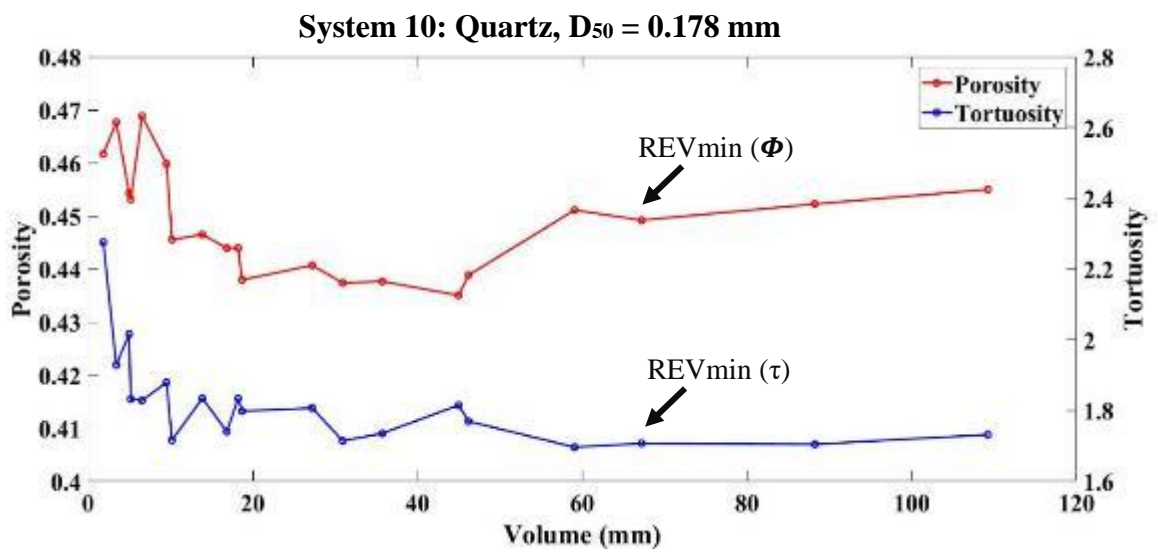


Figure 20. Distribution curve of porosity and tortuosity for system 10 marked with the REVmin values of both properties.

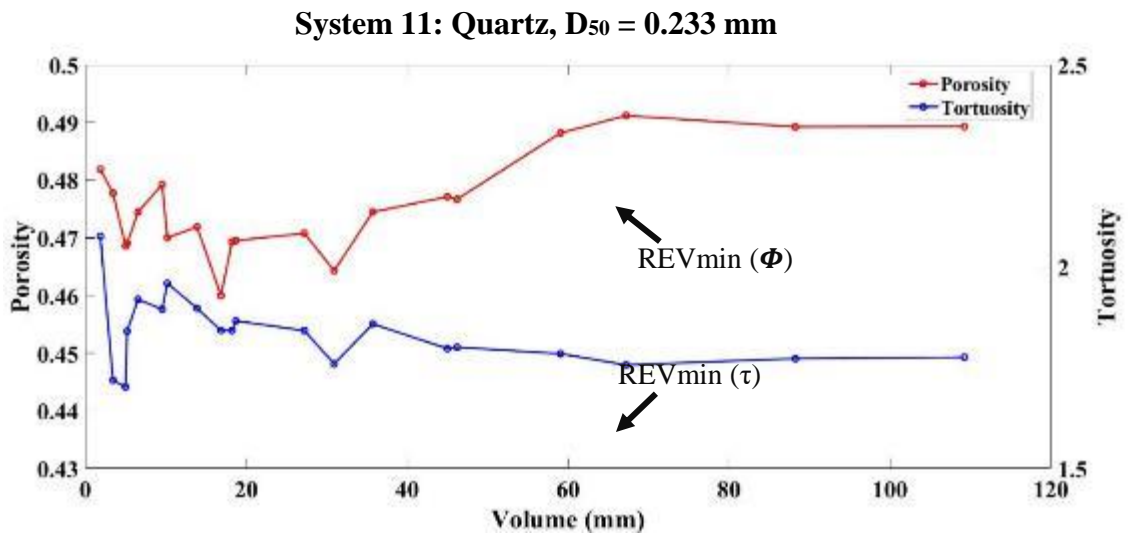


Figure 21. Distribution curve of porosity and tortuosity for system 11 marked with the REVmin values of both properties.

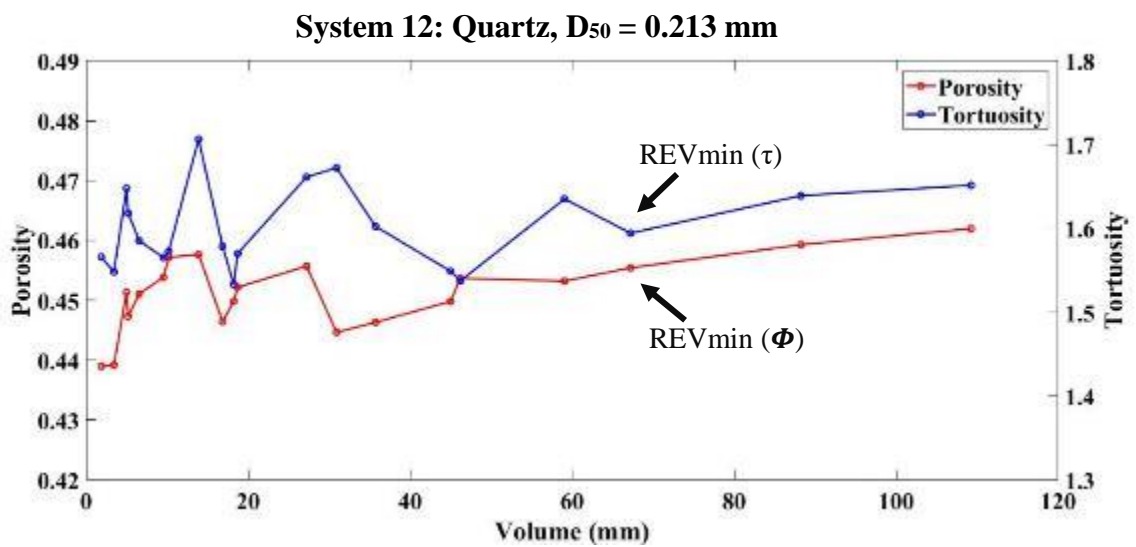


Figure 22. Distribution curve of porosity and tortuosity for system 12 marked with the REVmin values of both properties.

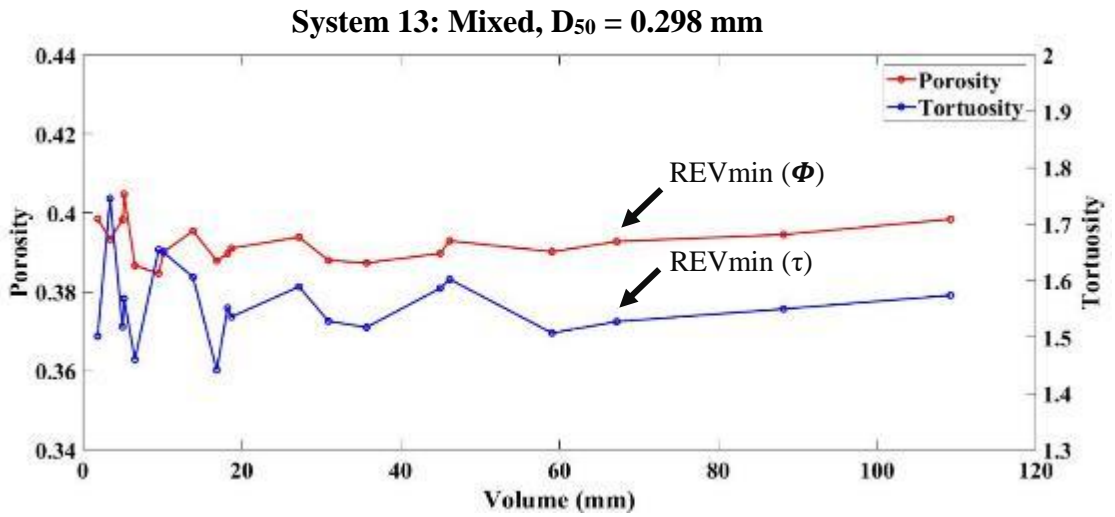


Figure 23. Distribution curve of porosity and tortuosity for system 13 marked with the REVmin values of both properties.

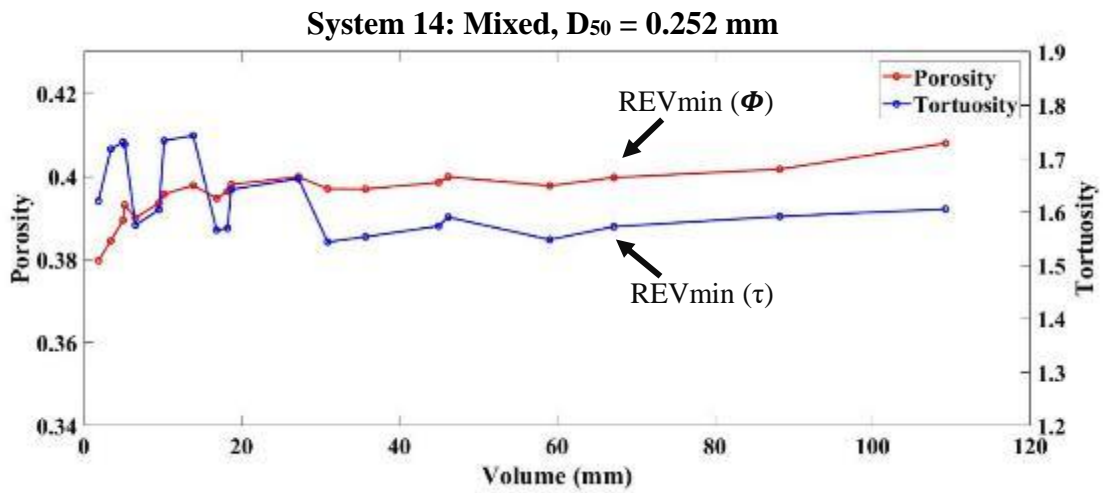


Figure 24. Distribution curve of porosity and tortuosity for system 14 marked with the REVmin values of both properties.

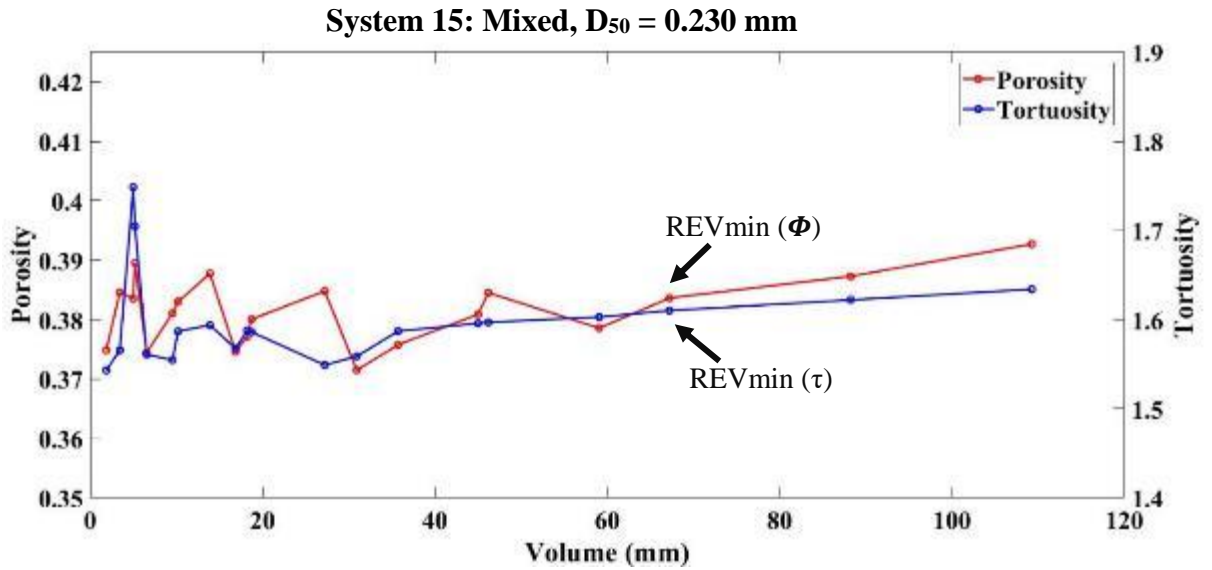


Figure 25. Distribution curve of porosity and tortuosity for system 15 marked with the REVmin values of both properties.

Micro-computed tomography is one of the sufficient technique that is used to provide cross-sectional views depending on the amount of x-ray absorbed. Moreover, it generates a high-resolution three-dimensional image to visualize the structure of porous media. Thus, computed tomography images were used to determine microscopic parameters such as porosity and tortuosity for each subvolume selected in each system. Moreover, for each system the distribution curve of porosity and tortuosity was potted as shown in figures (6-8), and the rest figures are presented in Appendix B. The variation in all figures for porosity and tortuosity while increasing the volume, at the beginning it fluctuated then it turns stagnant indicating the initiation of a REV region. In other words, the REV region always instigated, when the variation curve of porosity and tortuosity with the volume become almost a straight line. Therefore, this means that the REV region exists and it needs to be determined. Moreover, the initiation of this straight line always occurred at a point known as REVmin value. To obtain REVmin values, a MatLab code was developed to compute REV from 3D computed tomography

images. The REVmin values for both microscopic parameters were determined successfully using the developed MatLab code that is represented in the flow chart in Figure 9. Where the code is presented in Appendix C. The results demonstrated that the code successfully measured REVmin values for porosity and tortuosity as illustrated in figures 11-26. Where all computed values of REVmin volume values of porosity and tortuosity of each system (1-15) are summarized in table 4 as well as each distribution curve of each system is marked with the REVmin values of both properties as shown in figures (11-26).

Table 4. REVmin Volume Values of Porosity and Tortuosity for All Systems.

System #	REV_volume (Φ) (mm³)	REV_volume (τ) (mm³)
system 1	46.24	67.26
system 2	46.24	67.26
system 3	46.24	67.26
system 4	46.24	67.26
system 5	59.07	67.26
system 6	35.73	67.26
system 7	46.24	45.03
system 8	67.26	67.26
system 9	67.26	67.26
system 10	67.26	67.26
system 11	67.26	67.26
system 12	67.26	67.26
system 13	67.26	67.26
system 14	67.26	67.26
system 15	67.26	67.26

To visualize the difference between each value of REVmin (Φ) and REVmin (τ) for each system, two curve charts of REVmin volume of porosity and tortuosity for each system were plotted down below in figures 26, 27.

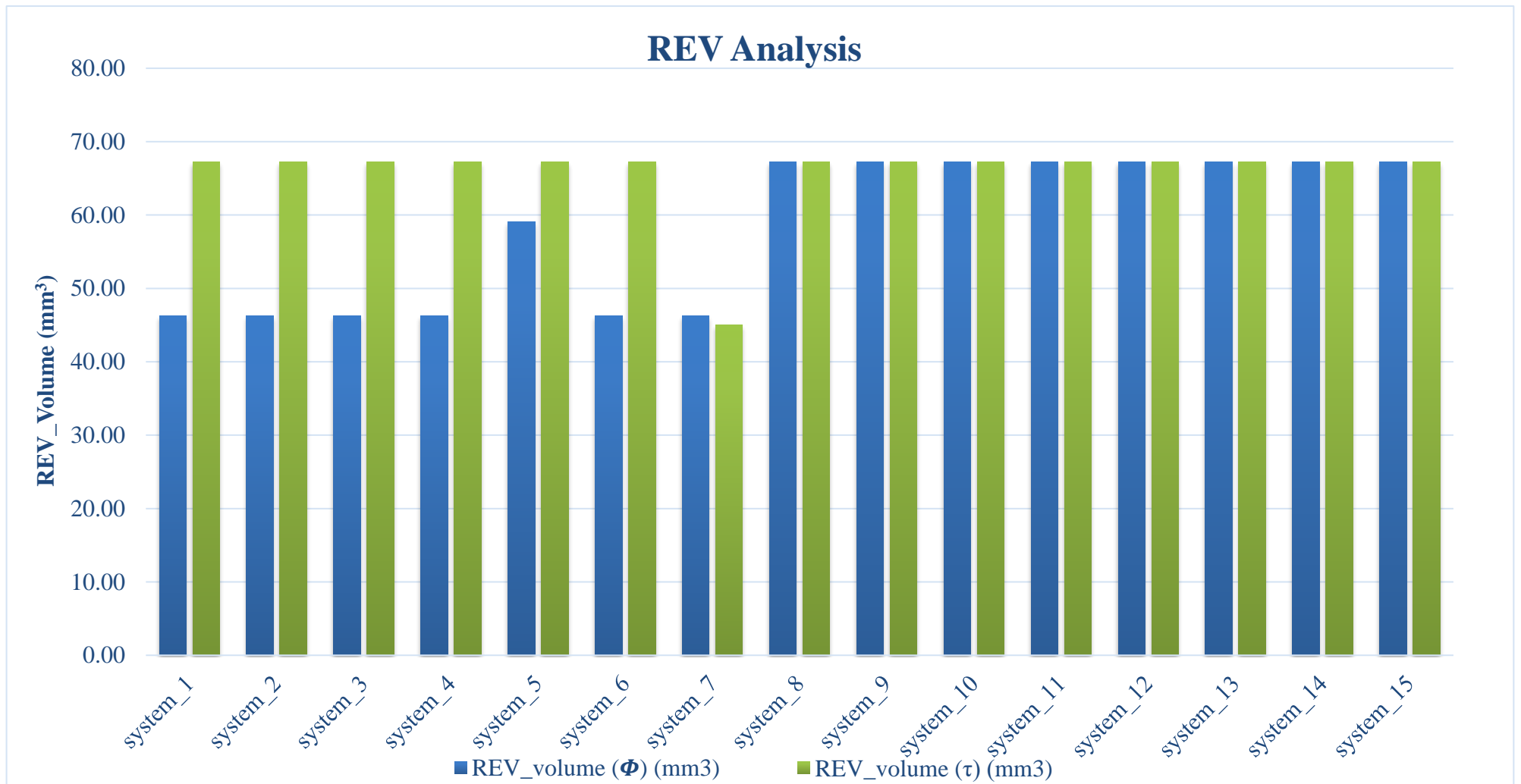


Figure 26. REVmin volume values of all systems (1-15) for both microscopic properties.

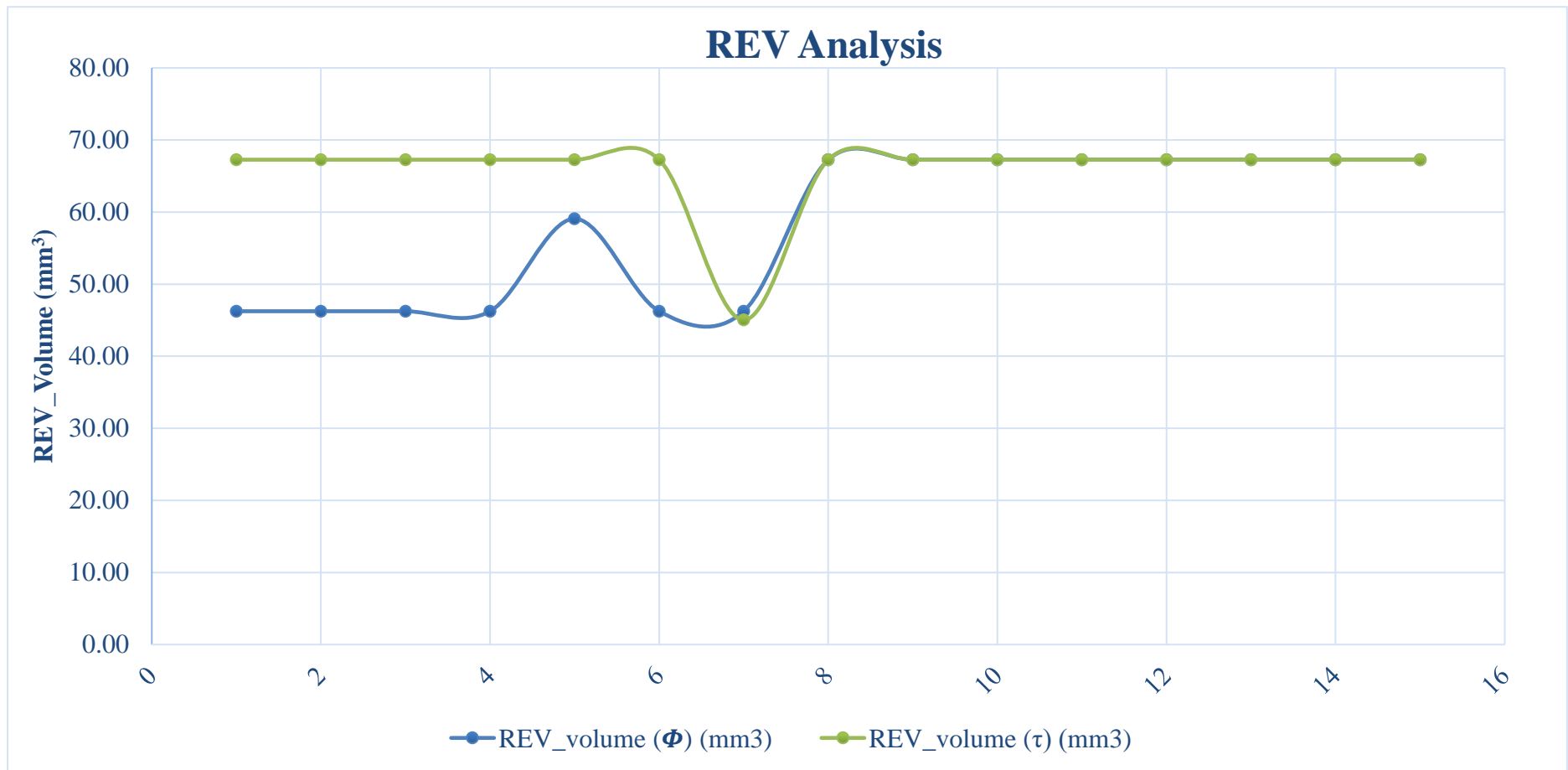


Figure 27. REVmin values for all systems (1-15) of both microscopic properties.

As shown in figures 26, 27 all values of REVmin volume were plotted in two different curve charts. In figure 26 at the beginning, system 1 through 6 are all characterized with silica geometry which is considered as regular shape; thus, sphericity and roundness index is almost higher than 0.8, where it ranges between (0.89 - 0.798) as illustrated in table 1. Moreover, the REVmin values for porosity less than REVmin values for tortuosity. In other words, it requires more volume for tortuosity to reach REV region than REV region for porosity. Whereas, system 7 through 12 are all characterized by quartz geometry which is considered as an irregular shape. Therefore, the sphericity and roundness index less than silica geometry, and it is observed that the REVmin values for porosity and tortuosity are equal. Thus, similar volume size is required to reach the REV region of both properties. Besides, this also was observed with the mixed systems of silica and quartz in system 13 through system 15, that both microscopic properties reach REV volume region at the same time. To visualize results more clearly, the same data was potted with different chart type as shown above in figure 27. Where at systems (1-6) the REV of porosity is lower than REV of tortuosity, then REV of porosity deviates and become equal to REV of tortuosity at system (7-15).

In general, REVmin values of porosity for silica geometry reaches REV region faster than for quartz and mixed geometry, meaning that for silica geometry it requires less volume. However, when the geometry changes to quartz or mixed between silica and quartz, the REVmin values of porosity increased where the volume needed to reach REV region is increased. Thus, it is observed that the REV for porosity is affected by the geometry of the media. On the other hand, REVmin for tortuosity generally constant regardless of the geometry of the media. Hence, REV for tortuosity is not affected by the geometry of the media. It is true because porosity is affected by pore space that is influenced by the geometry of the pore solid. Hence, having a regular spherical

geometry of the pore particle, the pore space will be higher. However, having an irregular geometry of the pore particle, the pore space will be smaller as visualized in figure 28 down below:

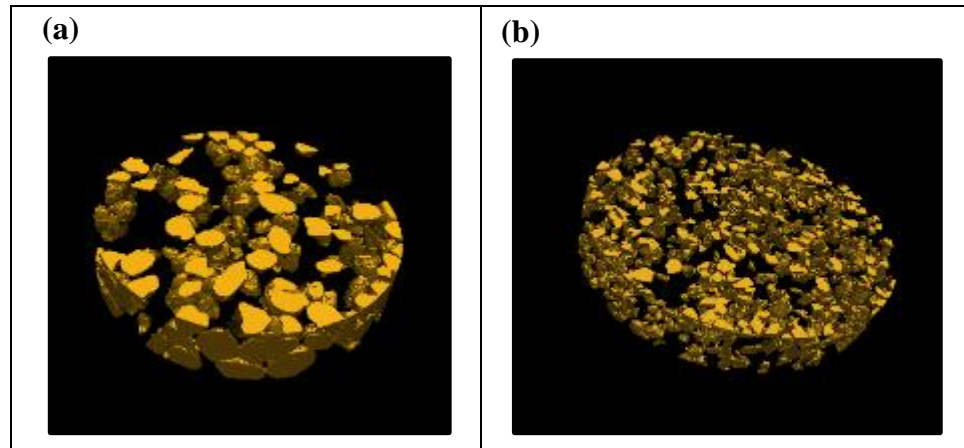


Figure 28. Showing pore space and pore particales of (a) 3D image of system 1 with silica particles geometry, and (b) 3D image of system 7 with quartz particles geometry.

Figure 28 demonstrated the pore space and pore particle of silica and quartz geometry, which is considered as regular and irregular geometries respectively. It is observed that for regular geometry higher pore space is shown compared with the irregular geometry.

Another important parameter that was analyzed is the normalized REVmin volume, which is merely a dimensionless parameter that is driven by dividing REVmin volume by the volume find at D_{50} . Where this gives the number of particles required to reach REV region. Table 5 summarized REVmin normalized volume values of porosity and tortuosity for all systems. In addition, these values were plotted in figures 29, 30.

Table 5. REVmin normalized Volume Values of Porosity and Tortosity for All Systems.

System #	REV_volume (Φ) (mm³)/volume(D₅₀)(mm³)	REV_volume (τ) (mm)/ volume(D₅₀)(mm³)
system 1	314.02	456.76
system 2	475.16	691.16
system 3	825.86	1201.28
system 4	1532.55	2229.23
system 5	1024.09	1166.08
system 6	683.45	1286.55
system 7	589.59	574.17
system 8	1124.21	1124.21
system 9	1524.65	1524.65
system 10	2702.88	2702.88
system 11	1577.45	1577.45
system 12	1887.59	1887.59
system 13	964.35	964.35
system 14	1348.55	1348.55
system 15	1618.87	1618.87

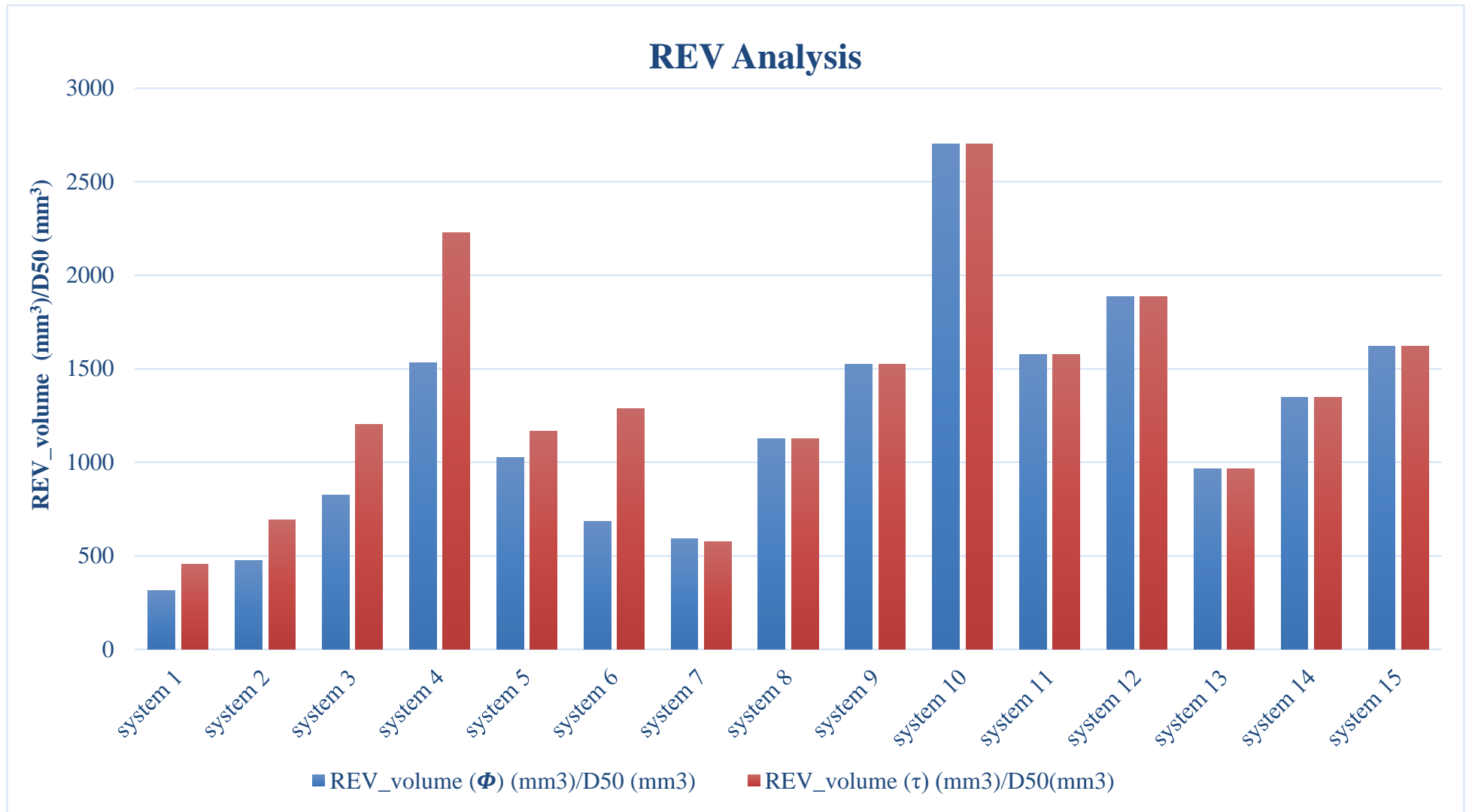


Figure 29. REVmin normalized volume values of all systems (1-15) for both microscopic properties.

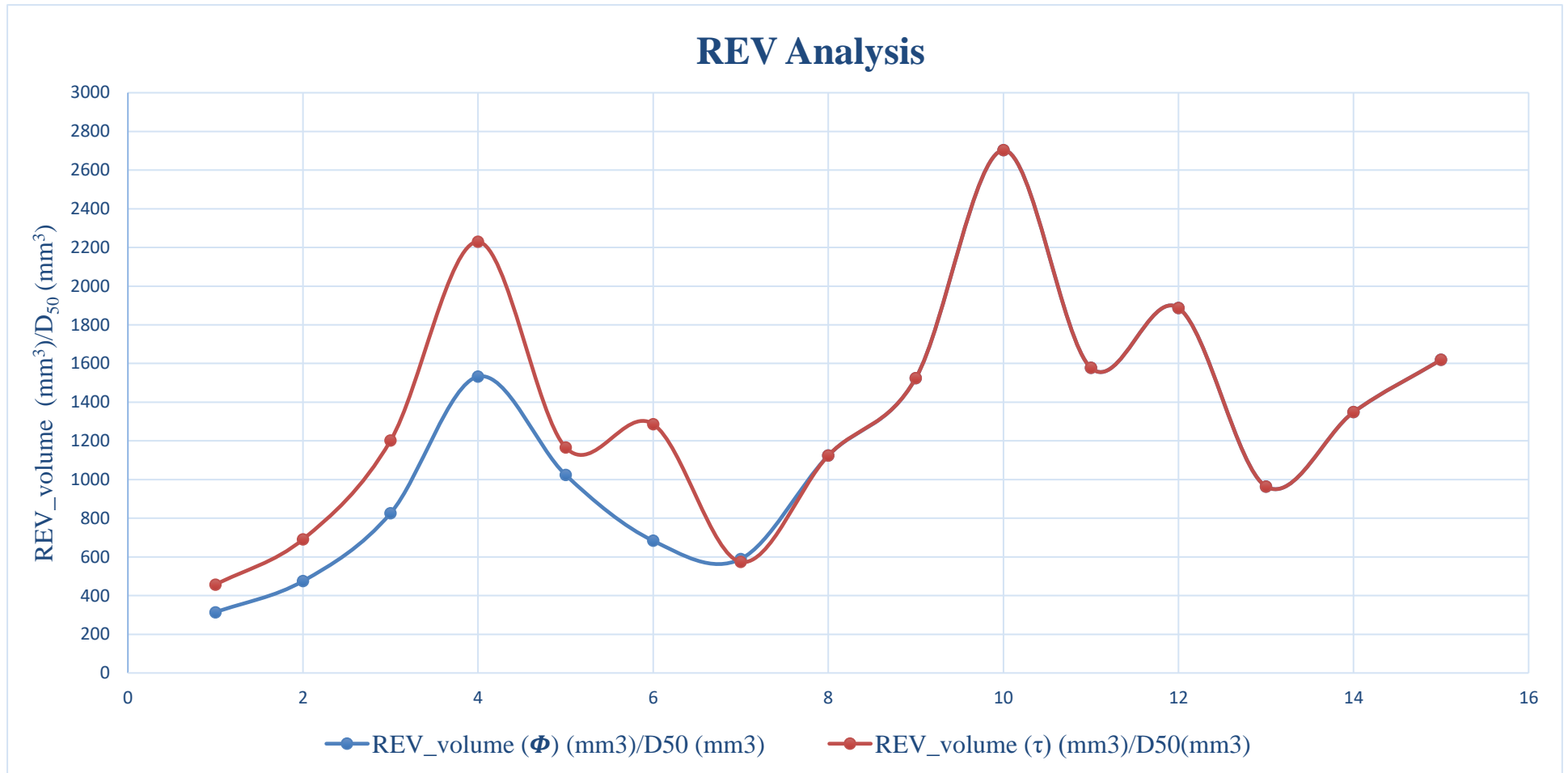


Figure 30. REVmin values for all systems (1-15) of both microscopic properties.

REVmin normalized volume values were calculated by dividing the REVmin volume by the volume at D_{50} . Where this analysis is more feasible as it gives the number of particles required reaching REV region. As shown above in figure 29 and 30, for regular geometry such as silica from system 1-6, almost the number of particles required to reach REV region of porosity is higher than the number of particles to reach REV region of tortuosity. Whereas, from system 7-15 that is characterized by irregular geometry such as quartz and mixtures of silica and quartz, almost equal number of particles required for reaching REV region of porosity and tortuosity. For instance, at system 4 the number of particles to reach REV region of porosity almost equal to 1500 particles. Whereas, the number of particles to reach REV region of tortuosity equal to 2200 particles. However, for system 12 equal number of particles required to reach REV region for porosity and tortuosity that is equal 1900 particles.

In overall, the relationship is interpreted by emphasizing that for silica and rounded geometry that is considered as regular geometry, REVmin for porosity is lower than REVmin for tortuosity. Besides, for quartz and non-rounded geometry that is considered as irregular geometry, the REVmin for porosity is equal to REVmin for tortuosity. The main conclusion is that having a REV of porosity is not sufficient to define a REV of tortuosity, as the REV of porosity is always lower than REV of tortuosity only when the geometry of the assigned porous media is rounded silica shape. However, when the geometry of porous media is quartz non-rounded or is mixed between silica and quartz, the REV of porosity is sufficient to define a REV of tortuosity. As reported in the literature, many studies attempted to use 3-dimensional images to find REV for porosity and tortuosity only for circular particles [113,120]. Although Wu et al and Sun et al. [113,120] found that REV of porosity is always lower than of tortuosity for only sphere geometry; however, in this study, the relationship

between REV of porosity and tortuosity was generalized as it was adopted for different porous media geometry and a wide range of grain sizes.

CHAPTER 5: CONCLUSION AND RECOMMENDATION

In this thesis, the representative elementary volumes (REV) of tortuosity and porosity were computed using three-dimensional microcomputed tomography images for fifteen natural sand systems. The data used was characterized by different geometry such as silica, quartz, and mixed sands, as well as, with a wide range of grain sizes. To the best knowledge, the novelty of this thesis is filling the gaps in the literature related to the lack in determining whether a REV for porosity is sufficient to define REV for tortuosity for different geometries at a wide range of grain sizes. Whereas, in literature, it was restricted only to sphere regular geometry. This study, therefore, has provided a comparison of REV of porosity and tortuosity for regular and irregular geometries, leading to a more realistic conclusion, as the real porous media is not characterized with a regular geometry. It was observed that REV_{min} value of tortuosity is not affected by the geometry of porous media. For instance, for irregular geometry, REV_{min} of tortuosity is almost constant. Whereas, the REV_{min} of porosity was fluctuated as for regular geometry the REV_{min} value was less than irregular. This means that it is affected by the geometry of the porous media. Moreover, this study also showed that for regular geometry, the REV of porosity is not sufficient to define REV of tortuosity. However, when the geometry of the media is irregular, the REV of porosity is sufficient to define the REV of tortuosity. As a future perspective, this work could be further enhanced by finding the limitation of the regularity of the geometry in which REV_{min} of porosity deviates to behave equally to REV_{min} of tortuosity. Additionally, an analytical relationship could be developed between REV_{min} (Φ) and REV_{min} (τ) depending on different parameters such as geometry, D_{50} , sphericity index (Ψ) and roundness index (X_v).

REFERENCES

- [1] M. Cieszko, Description of anisotropic pore space structure of permeable materials based on Minkowski metric space, *Arch. Mech.* 61 (2009) 425–444. doi:10.1093/sf/sow106.
- [2] A. Li, S. Payandeh, An Overview of Path Tortuosity Measures for Tracking and Monitoring, (2016) 294–297. doi:10.1016/j.vetimm.2006.02.010.
- [3] A. Yamasaki, An overview of CO₂mitigation options for global warming - Emphasizing CO₂sequestration options, *J. Chem. Eng. Japan.* 36 (2003) 361–375. doi:10.1252/jcej.36.361.
- [4] V. Joekar-Niasar, F. Doster, R.T. Armstrong, D. Wildenschild, M.A. Celia, Trapping and hysteresis in two-phase flow in porous media: A pore-network study, *Water Resour. Res.* 49 (2013) 4244–4256. doi:10.1002/wrcr.20313.
- [5] A. Khalili, B. Liu, K. Javadi, M.R. Morad, R. Stocker, Application of Porous Media Theories in Marine Biological Modeling, CRC Press, Boca Raton (FL), USA, 2010.
- [6] J. Cai, B. Yu, A Discussion of the Effect of Tortuosity on the Capillary Imbibition in Porous Media, *Transp. Porous Media.* 89 (2011) 251–263. doi:10.1007/s11242-011-9767-0.
- [7] B. Ghanbarian, A.G. Hunt, R.P. Ewing, M. Sahimi, Tortuosity in Porous Media: A Critical Review, *Soil Sci. Soc. Am. J.* 77 (2013) 1461. doi:10.2136/sssaj2012.0435.
- [8] V. Karanikola, A.F. Corral, H. Jiang, A.E. Sáez, W.P. Ela, R.G. Arnold, Effects of membrane structure and operational variables on membrane distillation performance, *J. Memb. Sci.* 524 (2017) 87–96. doi:10.1016/j.memsci.2016.11.038.

- [9] M.F. Hernández-López, J. Gironás, I. Braud, F. Suárez, J.F. Muñoz, Assessment of evaporation and water fluxes in a column of dry saline soil subject to different water table levels, *Hydrol. Process.* 28 (2014) 3655–3669. doi:10.1002/hyp.9912.
- [10] Y. Yuan, N. Gholizadeh Doonechaly, S. Rahman, An Analytical Model of Apparent Gas Permeability for Tight Porous Media, *Transp. Porous Media.* 111 (2016) 193–214. doi:10.1007/s11242-015-0589-3.
- [11] C. Masciopinto, D. Palmiotta, Flow and Transport in Fractured Aquifers: New Conceptual Models Based on Field Measurements, *Transp. Porous Media.* 96 (2013) 117–133. doi:10.1007/s11242-012-0077-y.
- [12] R.I. Al-Raoush, Experimental investigation of the influence of grain geometry on residual NAPL using synchrotron microtomography, *J. Contam. Hydrol.* 159 (2014) 1–10. doi:10.1016/j.jconhyd.2014.01.008.
- [13] N. Dal Ferro, L. Sartori, G. Simonetti, A. Berti, F. Morari, Soil macro- and microstructure as affected by different tillage systems and their effects on maize root growth, *Soil Tillage Res.* 140 (2014) 55–65. doi:10.1016/j.still.2014.02.003.
- [14] L.F. Pires, J.A.R. Borges, J.A. Rosa, M. Cooper, R.J. Heck, S. Passoni, W.L. Roque, Soil structure changes induced by tillage systems, *Soil Tillage Res.* 165 (2017) 66–79. doi:10.1016/j.still.2016.07.010.
- [15] Lal, R., Shukla, M.K., *Principles of Soil Physics*, CRC Press, New York, 2004.
- [16] P. Moldrup, T. Olesen, T. Komatsu, P. Schjønning, D.E. Rolston, Tortuosity, Diffusivity, and Permeability in the Soil Liquid and Gaseous Phases, *Soil Sci. Soc. Am. J.* 65 (2001) 613. doi:10.2136/sssaj2001.653613x.
- [17] Z. Matyka, Maciej., Khalili, Arzhang., & Koza, Tortuosity-porosity relation in porous media flow, *Phys. Rev. E.* 78 (2008). doi:10.1103/PhysRevE.78.026306.

- [18] L.M. Anovitz, D.R. Cole, Characterization and Analysis of Porosity and Pore Structures, *Rev. Mineral. Geochemistry.* 80 (2015) 61–164. doi:10.2138/rmg.2015.80.04.
- [19] J.R. Nimmo, Porosity and Pore Size Distribution, in: *Ref. Modul. Earth Syst. Environ. Sci.*, 2013. doi:10.1016/B978-0-12-409548-9.05265-9.
- [20] J. Hu, P. Stroeven, Local porosity analysis of pore structure in cement paste, *Cem. Concr. Res.* 35 (2005) 233–242. doi:10.1016/j.cemconres.2004.06.018.
- [21] A. Koponen, M. Kataja, J. Timonen, Permeability and effective porosity of porous media, 56 (1997) 3319–3325.
- [22] R. Liu, Y. Jiang, B. Li, X. Wang, A fractal model for characterizing fluid flow in fractured rock masses based on randomly distributed rock fracture networks, *Comput. Geotech.* 65 (2015) 45–55. doi:10.1016/j.compgeo.2014.11.004.
- [23] A. Mohajeri, G.A. Narsilio, P. Pivonka, D.W. Smith, Computers and Geotechnics Numerical estimation of effective diffusion coefficients for charged porous materials based on micro-scale analyses, *Comput. Geotech.* 37 (2010) 280–287. doi:10.1016/j.compgeo.2009.10.004.
- [24] A. Islam, T. Farhana, S. Chevalier, M. Soufiane, Multi-scale experimental and numerical simulation workflow of absolute permeability in heterogeneous carbonates, *J. Pet. Sci. Eng.* 173 (2019) 326–338. doi:10.1016/j.petrol.2018.10.031.
- [25] J. Bear, *Dynamics of fluids in porous media*, American Elsevier Pub, New York, 1972.
- [26] J. Bear, M.Y. Corapcioglu, *Mechanics of fluids in porous media*, in: *Trans. Am. Geophys. Union*, 1983: pp. 109–110. doi:10.1029/EO064i011p00109-02.
- [27] T. Patsahan, M. Holovko, W. Dong, *Fluids in porous media*, *J. Chem. Phys.* 134

- (2011). doi:10.1063/1.3532546.
- [28] B. Vik, K.E. Sylta, A. Skauge, Evaluation of representative elementary volume for a vuggy carbonate rock—Part: Porosity, permeability, and dispersivity., *J. Pet. Sci. Eng.* 112 (2013) 48–60. doi:10.1016/j.petrol.2013.10.023.
- [29] G.O. Brown, H.T. Hsieh, D.A. Lucero, Evaluation of laboratory dolomite core sample size using representative elementary volume concepts, *Water Resour. Res.* 36 (2000) 1199–1207.
- [30] M.S. Costanza-Robinson, B.D. Estabrook, D.F. Fouhey, Representative elementary volume estimation for porosity, moisture saturation, and air-water interfacial areas in unsaturated porous media: Data quality implications, *Water Resour. Res.* 47 (2011) 1–12. doi:10.1029/2010WR009655.
- [31] D. Zhang, R. Zhang, S. Chen, W. E. Soll, Pore scale study of flow in porous media: Scale dependancy, RVE, and statistical RVE, *Geophys. Res. Lett.* 27 (2000) 1195–1198. doi:10.1029/1999GL011101.
- [32] C.-R. M.S., Z. Z., H. E.J., E. B.D., L. M.H., Implications of surfactant-induced flow for miscible-displacement estimation of air-water interfacial areas in unsaturated porous media, *Environ. Sci. Technol.* 46 (2012) 11206–11212. doi:10.1021/es303003v.
- [33] J.H. Li, L.M. Zhang, Y. Wang, D.G. Fredlund, Permeability tensor and representative elementary volume of saturated cracked soil, *Can. Geotech. J.* 46 (2009) 928–942. doi:10.1139/T09-037.
- [34] M.S. Costanza-robinson, B.D. Estabrook, D.F. Fouhey, Representative elementary volume estimation for porosity , moisture saturation , and air-water interfacial areas in unsaturated porous media : Data quality implications, *Water Resour. Res.* 47 (2011) 1–12. doi:10.1029/2010WR009655.

- [35] R.H.J. Peerlings, N.A. Fleck, Numerical analysis of strain gradient effects in periodic media, *J. Phys. Iv.* 11 (2001) 153–160.
- [36] V. Clausnitzer, J.W. Hopmans, Determination of phase-volume fractions from tomographic measurements in two-phase systems, *Adv. Water Resour.* 22 (1999) 577–584. doi:10.1016/S0309-1708(98)00040-2.
- [37] V. Kouznetsova, M.G.D. Geers, W.A.M. Brekelmans, Multi-scale constitutive modelling of heterogeneous materials with a gradient-enhanced computational homogenization scheme, *Int. J. Numer. Methods Eng.* 54 (2002) 1235–1260. doi:10.1002/nme.541.
- [38] P. Muller, C Siegesmund, S., Blum, Evaluation of the representative porous media using X-ray computed tomography, *Powder Technol.* 200 (2011) 69–77.
- [39] R. Al-Raoush, A. Papadopoulos, Representative elementary volume analysis of porous media using X-ray computed tomography, *Powder Technol.* 200 (2010) 69–77. doi:10.1016/j.powtec.2010.02.011.
- [40] T. Kanit, S. Forest, I. Galliet, V. Mounoury, D. Jeulin, Determination of the size of the representative volume element for random composites: Statistical and numerical approach, *Int. J. Solids Struct.* 40 (2003) 3647–3679. doi:10.1016/S0020-7683(03)00143-4.
- [41] J. Bear, *Dynamics of fluids in porous media*, Dover, New York, 2002.
- [42] P.A.C. Raats, *Dynamics of Fluids in Porous Media*, *Soil Sci. Soc. Am. J.* 37 (1973) vi. doi:10.2136/sssaj1973.03615995003700040004x.
- [43] M. Wu, Z. Cheng, J. Wu, J. Wu, Estimation of representative elementary volume for DNAPL saturation and DNAPL-water interfacial areas in 2D heterogeneous porous media, *J. Hydrol.* 549 (2017) 12–26. doi:10.1016/j.jhydrol.2017.03.062.
- [44] D. Brian, B. Jacob, B., Carol, *Continuum Models for Contaminant Transport in*

- Fractured Porous Formations, *Water Resour. Res.* 24 (1988) 1225–1236.
- [45] O. Chapuis, M. Prat, M. Quintard, O. Guillot, N. Mayer, Two-phase flow and evaporation in model fibrous media Application to the gas diffusion layer of PEM fuel cells, *J. Power Sources.* 178 (2008) 258–268. doi:10.1016/j.jpowsour.2007.12.011.
- [46] K. Nordahl, P.S. Ringrose, Identifying the Representative Elementary Volume for Permeability in Heterolithic Deposits Using Numerical Rock Models, *Math. Geosci.* 40 (2008) 753. doi:10.1007/s11004-008-9182-4.
- [47] C.P. Fernandes, F.S. Magnani, P.C. Philippi, Pore scale study of flow in porous media : Scale dependency , REV , and statistical REV Dongxiao Lattice-Boltzmann, *Adv. Water Resour.* 51 (2013) 1734. doi:10.1149/1.1359196.
- [48] B. Nøttinger, The effective permeability of a heterogeneous porous medium, *Transp. Porous Media.* 15 (1994) 99–127. doi:10.1007/BF00625512.
- [49] S. Ahmed, T.M. Müller, M. Madadi, V. Calo, Drained pore modulus and Biot coefficient from pore-scale digital rock simulations, *Int. J. Rock Mech. Min. Sci.* 114 (2019) 62–70. doi:10.1016/j.ijrmmms.2018.12.019.
- [50] A.L. Herring, E.J. Harper, L. Andersson, A. Sheppard, B.K. Bay, Effect of fluid topology on residual nonwetting phase trapping : Implications for geologic CO₂ sequestration, *Adv. Water Resour.* 62 (2013) 47–58. doi:10.1016/j.advwatres.2013.09.015.
- [51] F. Cappa, J. Rutqvist, Modeling of coupled deformation and permeability evolution during fault reactivation induced by deep underground injection of CO₂, *Int. J. Greenh. Gas Control.* 5 (2011) 336–346. doi:10.1016/j.ijggc.2010.08.005.
- [52] J.T. Birkholzer, Q. Zhou, C. Tsang, Large-scale impact of CO₂ storage in deep

- saline aquifers : A sensitivity study on pressure response in stratified systems, *Int. J. Greenh. Gas Control.* 3 (2009) 181–194. doi:10.1016/j.ijggc.2008.08.002.
- [53] R.I. Al-raoush, C.S. Willson, A pore-scale investigation of a multiphase porous media system, *Contam. Hydrol.* 77 (2005) 67–89. doi:10.1016/j.jconhyd.2004.12.001.
- [54] Q.C.H. Wu, S.S.Z. Yin, Protection of neighbour buildings due to construction of shield tunnel in mixed ground with sand over weathered granite, *Environ. Earth Sci.* 75 (2016) 1–11. doi:10.1007/s12665-016-5300-7.
- [55] V.A. Bakshevskaya, S.P. Pozdniakov, Simulation of Hydraulic Heterogeneity and Upscaling Permeability and Dispersivity in Sandy-Clay Formations, *Math. Geosci.* (2016) 45–64. doi:10.1007/s11004-015-9590-1.
- [56] M. Rezaei, T. Saey, P. Seuntjens, I. Joris, W. Boëne, M. Van Meirvenne, W. Cornelis, Predicting saturated hydraulic conductivity in a sandy grassland using proximally sensed apparent electrical conductivity, *J. Appl. Geophys.* 126 (2016) 35–41. doi:10.1016/j.jappgeo.2016.01.010.
- [57] S. Mohammad, H. Jazayeri, N. Cartwright, P. Nielsen, P. Perrochet, The effects of oscillation period on groundwater wave dispersion in a sandy unconfined aquifer : Sand flume experiments and modelling, *J. Hydrol.* 533 (2016) 412–420. doi:10.1016/j.jhydrol.2015.12.032.
- [58] W.M. Dijk, A.L. Densmore, A. Singh, S. Gupta, R. Sinha, P.J. Mason, S.K. Joshi, N. Nayak, M. Kumar, S. Shekhar, D. Kumar, S.P. Rai, Earth Surface Linking the morphology of fluvial fan systems to aquifer stratigraphy in the Sutlej-Yamuna plain of northwest India, *J. Geophys. Res. Earth Surface.* 121 (2016) 201–222. doi:10.1002/2015JF003720.
- [59] M. Sahimi, Flow phenomena in rocks : from continuum models to fractals ,

- percolation , cellular automata , and simulated annealing, *Rev. Mod. Phys.* 65 (1993).
- [60] L.F. Gladden, J. Mitchell, J. Korb, O. Neudert, S. Stapf, M. Wear, B. Studies, Focus on the physics of magnetic resonance on porous media, *New J. Phys.* (2012). doi:10.1088/1367-2630/14/5/055017.
- [61] S. Torquato, Statistical description of microstructures, *Annu. Rev. Mater. Res.* 32 (2002) 77–111. doi:10.1146/annurev.matsci.32.110101.155324.
- [62] L.M. Keller, L. Holzer, P. Schuetz, P. Gasser, Pore space relevant for gas permeability in Opalinus clay : Statistical analysis of homogeneity , percolation , and representative volume element, *Geophys. Res. Solid Earth.* 118 (2013) 2799–2812. doi:10.1002/jgrb.50228.
- [63] D. Müter, H.O. Sørensen, D. Jha, R. Harti, K.N. Dalby, H. Suhonen, R. Feidenhans, F. Engstrøm, Resolution dependence of petrophysical parameters derived from X-ray tomography of chalk, *Appl. Phys. Lett.* (2014) 1–6. doi:10.1063/1.4891965.
- [64] S. Saraji, M. Piri, The representative sample size in shale oil rocks and nano-scale characterization of transport properties, *Int. J. Coal Geol.* 146 (2015) 42–54. doi:10.1016/j.coal.2015.04.005.
- [65] Y. Bachmat, J. Bear, Macroscopic Modelling of Transport Phenomena in Porous Media . 1 : The Continuum Approach, *Transp. Porous Media.* 1 (1986) 213–240.
- [66] M. Barrande, R. Bouchet, R. Denoyel, Tortuosity of Porous Particles, *Anal. Chem.* 79 (2007) 9115–9121. doi:10.1021/ac071377r.
- [67] L. Pisani, Simple Expression for the Tortuosity of Porous Media, *Transp. Porous Media.* 88 (2011) 193–203. doi:10.1007/s11242-011-9734-9.
- [68] S.S. Manickam, J. Gelb, J.R. Mccutcheon, Pore structure characterization of

- asymmetric membranes : Non-destructive characterization of porosity and tortuosity, *J. Memb. Sci.* 454 (2014) 549–554. doi:10.1016/j.memsci.2013.11.044.
- [69] P. Lanfrey, Z. V Kuzeljevic, M.P. Dudukovic, Tortuosity model for fixed beds randomly packed with identical particles, *Chem. Eng. Sci.* 65 (2010) 1891–1896. doi:10.1016/j.ces.2009.11.011.
- [70] L.I. Jian-hua, Y.U. Bo-ming, Tortuosity of Flow Paths through a Sierpinski Carpet, *Chinese Phys. Lett.* 28 (2011) 4–6. doi:10.1088/0256-307X/28/3/034701.
- [71] J.P.D.U. Plessis, J.H. Masliyah, Flow Through Isotropic Granular Porous Media, *Transp. Porous Media.* 6 (1991) 207–221.
- [72] A. Duda, Z. Koza, M. Matyka, Hydraulic tortuosity in arbitrary porous media flow, *Phys. Rev. E.* 84 (2011) 1–8. doi:10.1103/PhysRevE.84.036319.
- [73] I. Freytag, W.L. Roque, Influence of granular packing on porosity and tortuosity, *Phys. Rev. E.* 88 (2013) 1–6. doi:10.1103/PhysRevE.88.023011.
- [74] M.M. Ahmadi, S. Mohammadi, A.N. Hayati, Analytical derivation of tortuosity and permeability of monosized spheres : A volume averaging approach, 026312 (2011) 1–8. doi:10.1103/PhysRevE.83.026312.
- [75] H. Takahashi, Y. Seida, M. Yui, 3D X-ray CT and diffusion measurements to assess tortuosity and constrictivity in a sedimentary rock, *Diffus Fundam.* 11 (2009) 1–11.
- [76] R.P. Udawatta, C.J. Gantzer, S.H. Anderson, A.M. Rossi, R.C. Graham, R.A. Ketcham, Analysis of Three-dimensional Geometrical Pore Parameters From Rock Weathering, *Soil Sci.* 177 (2012) 506–516. doi:10.1097/SS.0b013e31825f20c6.

- [77] S. Pardo-alonso, J. Vicente, E. Solórzano, M.Á. Rodríguez-, D. Lehmus, Geometrical tortuosity 3D calculations in infiltrated aluminium cellular materials, *Procedia Mater. Sci.* 4 (2014) 145–150. doi:10.1016/j.mspro.2014.07.553.
- [78] N.O. Shanti, V.W.L. Chan, S.R. Stock, F. De Carlo, K. Thornton, K.T. Faber, X-ray micro-computed tomography and tortuosity calculations of percolating pore networks, *Acta Mater.* 71 (2014) 126–135. doi:10.1016/j.actamat.2014.03.003.
- [79] M. Naveed, S. Hamamoto, K. Kawamoto, T. Sakaki, M. Takahashi, T. Komatsu, P. Moldrup, M. Lamande, D. Wildenschild, Correlating Gas Transport Parameters and X-Ray Computed Tomography Measurements in Porous Media, *Soil Sci.* 178 (2013) 60–68. doi:10.1097/SS.0b013e318288784c.
- [80] M.A.B. Promentilla, T. Sugiyama, T. Hitomi, N. Takeda, Cement and Concrete Research Quantification of tortuosity in hardened cement pastes using synchrotron-based X-ray computed microtomography, *Cem. Concr. Res.* 39 (2009) 548–557. doi:10.1016/j.cemconres.2009.03.005.
- [81] R.I. Al-raoush, I.T. Madhoun, TORT3D: A MATLAB code to compute geometric tortuosity from 3D images of unconsolidated porous media, *Powder Technol.* 320 (2017) 99–107. doi:10.1016/j.powtec.2017.06.066.
- [82] P. Evesque, Fluctuations, Correlation and Representative Elementary Volume (REV) in Granular Materials, 17 (2000) 6–17.
- [83] M.D. Jackson, S. Yoshida, A.H. Muggeridge, H.D. Johnson, Three-dimensional reservoir characterization and flow simulation of heterolithic tidal sandstones, 4 (2005) 507–528. doi:10.1306/11230404036.
- [84] M.D. Jackson, S. Yoshida, A.H. Muggeridge, H.D. Johnson, Upscaling

- Permeability Measurements Within Complex Heterolithic Tidal Sandstones, *Math. Geol.* 35 (2003) 499–520. doi:doi:10.1023/a:1026236401104.
- [85] S. H, A.A. Carter, P. Dranfield, Assigning Effective Values to Simulator Gridblock Parameters for Heterogeneous Reservoirs, *SPE Reserv. Eng.* 4 (1989) 455–463. doi:doi:10.2118/16754-pa.
- [86] C. Deutsch, U. Stanford, Calculating Effective Absolute Permeability in Sandstone / Shale Sequences, *SPE Form. Eval.* 4 (1989) 343–348. doi:doi:10.2118/17264-pa.
- [87] E.F. Wood, M. Sivapalan, K. Beven, L. Band, Effects of Spatial Variability and Scale With Implications to Hydrologic Modeling, *J. Hydrol.* 102 (1988) 29–47. doi:10.1016/0022-1694(88)90090-X.
- [88] B. Buchter, C. Hinz, H. Flthler, Sample size for determination of coarse fragment content in a stony soil, *Geoderma.* 63 (1994) 265–275. doi:doi:10.1016/0016-7061(94)90068-x.
- [89] A.J. Vandenbygaart, R. Protz, A.D. Tomlin, J.J. Miller, Tillage system effects on near-surface soil morphology: observations from the landscape to micro-scale in silt loam soils of southwestern Ontario, *Soil Tillage Res.* 51 (1999) 139–149.
- [90] J.A.R. Borges, L.F. Pires, J.C. Costa, Representative Elementary Length to Measure Soil Mass Attenuation Coefficient, *Sci. World.* (2014) 1–9. doi:doi:10.1155/2014/584871.
- [91] T. Nguyen, G. Combe, D. Caillerie, J. Desrues, FEM×DEM Modelling of Cohesive Granular Materials: Numerical Homogenisation and Multi-scale Simulations, *Acta Geophys.* 62 (2014) 1109–1126. doi:10.2478/s11600-014-0228-3.

- [92] J. Wi, M. Molenda, Representative elementary volume analysis of polydisperse granular packings using discrete element method, *Particuology*. (2015). doi:10.1016/j.partic.2015.08.004.
- [93] M. Andrew, B. Bijeljic, M.J. Blunt, Pore-by-pore capillary pressure measurements using X-ray microtomography at reservoir conditions: Curvature, snap-off, and remobilization of residual CO₂, *Water Resour. Res.* (2014) 8760–8774. doi:10.1002/2014WR015970.Received.
- [94] T. Mukunoki, Y. Miyata, K. Mikami, E. Shiota, X-ray CT analysis of pore structure in sand, (2016) 929–942. doi:10.5194/se-7-929-2016.
- [95] G.N. Hounsfield, Computerized transverse axial scanning (tomography): Part I. Description of system, *Br. J. Radiol.* 46 (1973) 1016–1022. doi:doi:10.1259/0007-1285-46-552-1016.
- [96] M. Andrew, B. Bijeljic, M.J. Blunt, Pore-scale contact angle measurements at reservoir conditions using X-ray microtomography, *Adv. Water Resour.* 68 (2014) 24–31. doi:10.1016/j.advwatres.2014.02.014.
- [97] C.S. Al-Raoush, R.I. Willson, Extraction of physically realistic pore network properties from three-dimensional synchrotron X-ray microtomography images of unconsolidated porous media systems, *J. Hydrol.* 300 (2005) 44–64. doi:10.1016/j.jhydrol.2004.05.005.
- [98] K.A. Culligan, D. Wildenschild, B.S.B. Christensen, Pore-scale characteristics of multiphase flow in porous media : A comparison of air – water and oil – water experiments, *Adv. Water Resour.* 29 (2006) 227–238. doi:10.1016/j.advwatres.2005.03.021.
- [99] V. Pot, S. Peth, O. Monga, L.E. Vogel, A. Genty, P. Garnier, L. Vieublé-gonod, M. Ogurreck, F. Beckmann, P.C. Baveye, Three-dimensional distribution of

- water and air in soil pores : Comparison of two-phase two-relaxation-times lattice-Boltzmann and morphological model outputs with synchrotron X-ray computed tomography data, *Adv. Water Resour.* 84 (2015) 87–102. doi:10.1016/j.advwatres.2015.08.006.
- [100] J.A.R. Borges, L.F. Pires, F.A.M. Cássaro, W.L. Roque, R.J. Heck, J.A. Rosa, F.G. Wolf, X-ray microtomography analysis of representative elementary volume (REV) of soil morphological and geometrical properties, *Soil Tillage Res.* 182 (2018) 112–122. doi:10.1016/j.still.2018.05.004.
- [101] A. Pedrotti, E.A. Pauletto, S. Crestana, P.E. Cruvinel, M.P. Vaz, J.D.M. Naime, A. Macedo, Planosol Soil Sample Size For Computerized Tomography Measurement Of Physical Parameters, *Sci. Agric.* 60 (2003) 735–740.
- [102] P. Baveye, H. Rogasik, O. Wendroth, I. Onasch, J.W. Crawford, Effect of sampling volume on the measurement of soil physical properties : simulation with x-ray tomography data, *Meas. Sci. Technol.* 13 (2002) 775–784. doi:10.1088/0957-0233/13/5/316.
- [103] T.R. Ferreira, J.A.R. Borges, L.F. Pires, Representative elementary area for soil bulk density measurements of samples collected in volumetric rings by CT image analyses, *Soil Tillage Res.* 152 (2015) 74–84. doi:10.1016/j.still.2015.03.007.
- [104] N.D. Ferro, P. Delmas, C. Duwig, G. Simonetti, F. Morari, Coupling X-ray microtomography and mercury intrusion porosimetry to quantify aggregate structures of a cambisol under different fertilisation treatments, *Soil Tillage Res.* 119 (2012) 13–21. doi:10.1016/j.still.2011.12.001.
- [105] D.A. Jefferies, R.J. Heck, Characterizing soil surface structure in a temperate tree-based intercropping system using X-ray computed tomography, *Agrofor.*

Syst. 88 (2014) 645–656. doi:10.1007/s10457-014-9699-0.

- [106] L.F. Pires, J.A.R. Borges, O.O.S. Bacchi, K. Reichardt, Soil & Tillage Research Twenty-five years of computed tomography in soil physics : A literature review of the Brazilian contribution, Soil Tillage Res. 110 (2010) 197–210. doi:10.1016/j.still.2010.07.013.
- [107] O.M.O. de Araújo, K. V Sharma, A.S. Machado, T.M.P. Santos, C.G. Ferreira, R. Straka, F.W. Tavares, R.T. Lopes, Representative elementary volume in limestone sample, J. Instrum. 13 (2018). doi:doi:10.1088/1748-0221/13/10/c10003.
- [108] S.M. Shah, J.P. Crawshaw, F. Gray, J. Yang, E.S. Boek, Convex hull approach for determining rock representative elementary volume for multiple petrophysical parameters using pore-scale imaging and Lattice–Boltzmann modelling, Adv. Water Resour. 104 (2017) 65–75. doi:10.1016/j.advwatres.2017.03.008.
- [109] A.S. Al-Kharusi, M.J. Blunt, Network extraction from sandstone and carbonate pore space images, J. Pet. Sci. Eng. 56 (2007) 219–231. doi:10.1016/j.petrol.2006.09.003.
- [110] D. Silin, L. Tomutsa, S.M. Benson, T.W. Patzek, Microtomography and Pore-Scale Modeling of Two-Phase Fluid Distribution, Transp. Porous Media. 86 (2011) 495–515. doi:10.1007/s11242-010-9636-2.
- [111] C. Manwart, U. Aaltosalmi, A. Koponen, R. Hilfer, J. Timonen, Lattice-Boltzmann and finite-difference simulations for the permeability for three-dimensional porous media, Phys. Rev. E. 66 (2002) 1–11. doi:10.1103/PhysRevE.66.016702.
- [112] P. Mostaghimi, M. J. Blunt, B. Bijeljic, Computations of Absolute Permeability

- on Micro-CT Images, *Math. Geosci.* 45 (2013) 103–125. doi:10.1007/s11004-012-9431-4.
- [113] Z. Sun, X. Tang, G. Cheng, Numerical simulation for tortuosity of porous media
Zufeng, *Microporous Mesoporous Mater.* 173 (2013) 37–42.
doi:10.1016/j.micromeso.2013.01.035.
- [114] L. Luo, B. Yu, J. Cai, X. Zeng, Numerical simulation of tortuosity for fluid flow
in two-dimensional pore fractal models of porous media, *Fractals*. 22 (2014) 1–
7. doi:10.1142/S0218348X14500157.
- [115] A.N. Hayati, M.M. Ahmadi, S. Mohammadi, How particle shape affects the flow
through granular materials, *Phys. Rev. E.* 85 (2012) 3–6.
doi:10.1103/PhysRevE.85.036310.
- [116] M.R. Niemet, J.S. Selker, A new method for quantification of liquid saturation in
2D translucent porous media systems using light transmission, *Adv. Water
Resour.* 24 (2001) 651–666.
- [117] M.M. Bob, M.C. Brooks, S.C. Mravik, A.L. Wood, A modified light
transmission visualization method for DNAPL saturation measurements in 2-D
models, *Adv. Water Resour.* 31 (2008) 727–742.
doi:10.1016/j.advwatres.2008.01.016.
- [118] M. Wu, Z. Cheng, J. Wu, J. Wu, Quantifying representative elementary volume
of connectivity for translucent granular materials by light transmission micro-
tomography, *J. Hydrol.* 545 (2017) 12–27. doi:10.1016/j.jhydrol.2016.11.063.
- [119] M. Wu, J. Wu, J. Wu, Simulation of DNAPL migration in heterogeneous
translucent porous media based on estimation of representative elementary
volume, *J. Hydrol.* 553 (2017) 276–288. doi:10.1016/j.jhydrol.2017.08.005.
- [120] M. Wu, J. Wu, J. Wu, B.X. Hu, A three-dimensional model for quantification of

the representative elementary volume of tortuosity in granular porous media, J. Hydrol. 557 (2018) 128–136. doi:10.1016/j.jhydrol.2017.12.030.

APPENDIX

Appendix A: Tables for porosity and tortuosity values

Volume (mm)	System_1		System_2	
	Porosity	Tortuosity	Porosity	Tortuosity
109.26	0.327	1.497	0.356	1.467
88.24	0.327	1.507	0.354	1.469
67.22	0.326	1.546	0.353	1.455
59.07	0.331	1.446	0.351	1.464
46.2	0.327	1.496	0.352	1.439
45	0.329	1.457	0.350	1.447
35.73	0.332	1.555	0.353	1.416
30.93	0.328	1.552	0.349	1.429
27.22	0.332	1.518	0.353	1.435
18.71	0.330	1.570	0.351	1.404
18.23	0.331	1.538	0.355	1.401
16.86	0.333	1.487	0.348	1.416
13.89	0.332	1.638	0.353	1.389
10.2	0.334	1.416	0.350	1.432
9.55	0.334	1.730	0.352	1.369
6.56	0.337	1.637	0.357	1.412
5.2	0.336	1.448	0.354	1.382
5	0.340	1.699	0.357	1.397
3.44	0.332	1.821	0.356	1.397
1.87	0.340	1.653	0.359	1.391

Volume (mm)	System_3		System_4	
	Porosity	Tortuosity	Porosity	Tortuosity
109.26	0.382	1.392	0.330	1.419
88.24	0.380	1.384	0.329	1.413
67.22	0.379	1.385	0.327	1.418
59.07	0.378	1.407	0.327	1.450
46.2	0.378	1.379	0.326	1.413
45	0.376	1.399	0.325	1.424
35.73	0.379	1.420	0.330	1.398
30.93	0.375	1.397	0.325	1.390
27.22	0.378	1.415	0.328	1.420

18.71	0.378	1.392	0.327	1.415
18.23	0.380	1.422	0.331	1.409
16.86	0.374	1.412	0.325	1.391
13.89	0.379	1.432	0.328	1.419
10.2	0.377	1.386	0.327	1.406
9.55	0.379	1.413	0.327	1.407
6.56	0.381	1.442	0.333	1.371
5.2	0.378	1.411	0.328	1.355
5	0.378	1.434	0.331	1.398
3.44	0.378	1.427	0.340	1.401
1.87	0.376	1.374	0.337	1.319

Volume (mm)	System5		System6	
	Porosity	Tortuosity	Porosity	Tortuosity
109.26	0.323	1.485	0.369	1.488
88.24	0.323	1.472	0.367	1.487
67.22	0.323	1.465	0.367	1.498
59.07	0.315	1.501	0.368	1.450
46.2	0.322	1.473	0.366	1.461
45	0.314	1.530	0.368	1.504
35.73	0.315	1.473	0.369	1.467
30.93	0.312	1.537	0.368	1.453
27.22	0.315	1.487	0.370	1.482
18.71	0.311	1.451	0.369	1.442
18.23	0.317	1.507	0.368	1.644
16.86	0.316	1.462	0.370	1.430
13.89	0.316	1.527	0.371	1.685
10.2	0.315	1.467	0.373	1.449
9.55	0.311	1.441	0.372	1.477
6.56	0.310	1.499	0.362	1.501
5.2	0.317	1.437	0.379	1.447
5	0.308	1.484	0.367	1.492
3.44	0.305	1.628	0.365	1.491
1.87	0.306	1.551	0.369	1.468

Volume (mm)	System7		System8	
	Porosity	Tortuosity	Porosity	Tortuosity
109.26	0.470	1.967	0.488	1.640
88.24	0.469	1.924	0.484	1.618
67.22	0.466	1.915	0.482	1.637
59.07	0.467	1.947	0.486	1.631
46.2	0.465	1.941	0.481	1.605
45	0.464	1.939	0.484	1.641
35.73	0.470	2.085	0.488	1.724
30.93	0.466	1.925	0.483	1.589
27.22	0.468	2.057	0.485	1.750
18.71	0.468	2.098	0.486	1.684
18.23	0.474	1.890	0.489	1.650
16.86	0.465	1.943	0.483	1.588
13.89	0.470	1.912	0.488	1.700
10.2	0.468	2.003	0.484	1.588
9.55	0.460	1.958	0.491	1.691
6.56	0.482	2.491	0.481	1.730
5.2	0.453	2.101	0.488	1.673
5	0.475	2.378	0.479	1.674
3.44	0.469	2.084	0.487	1.758
1.87	0.475	1.609	0.486	1.533

Volume (mm)	System_9		System_10	
	Porosity	Tortuosity	Porosity	Tortuosity
109.26	0.505	1.527	0.455	1.732
88.24	0.499	1.524	0.452	1.704
67.22	0.494	1.520	0.449	1.707
59.07	0.489	1.550	0.439	1.769
46.2	0.492	1.533	0.451	1.696
45	0.485	1.547	0.435	1.815
35.73	0.490	1.564	0.441	1.807
30.93	0.481	1.551	0.438	1.735
27.22	0.487	1.553	0.438	1.798
18.71	0.483	1.584	0.444	1.834
18.23	0.494	1.626	0.447	1.834
16.86	0.481	1.544	0.437	1.714
13.89	0.492	1.664	0.446	1.716
10.2	0.484	1.584	0.444	1.740

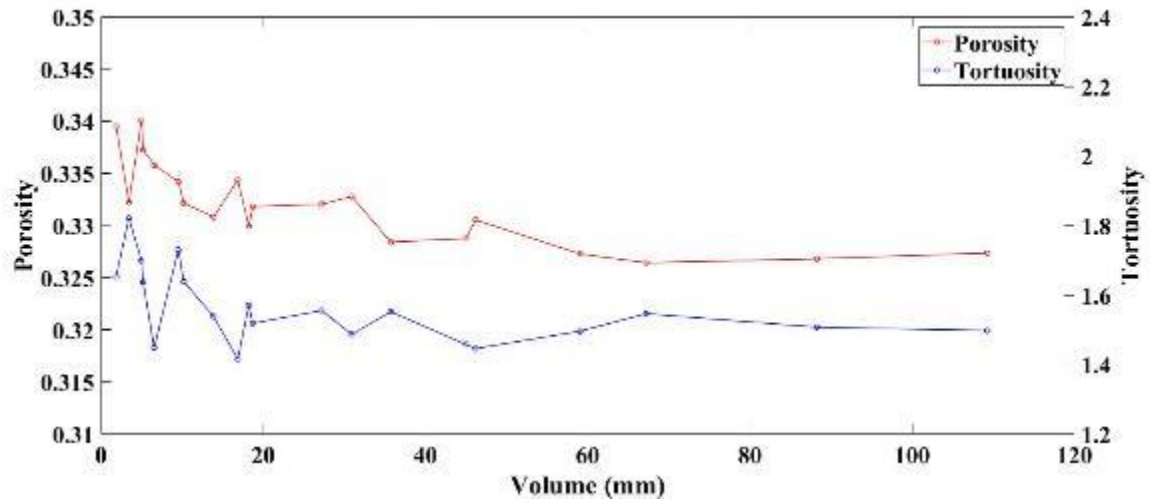
9.55	0.489	1.693	0.460	1.880
6.56	0.492	1.585	0.453	1.832
5.2	0.493	1.618	0.469	1.828
5	0.491	1.650	0.454	2.016
3.44	0.492	1.682	0.468	1.928
1.87	0.492	1.567	0.462	2.276

Volume (mm)	System11		System12	
	Porosity	Tortuosity	Porosity	Tortuosity
109.26	0.489	1.776	0.462	1.652
88.24	0.489	1.772	0.459	1.639
67.22	0.491	1.756	0.455	1.594
59.07	0.477	1.800	0.454	1.538
46.2	0.488	1.784	0.453	1.635
45	0.477	1.797	0.450	1.549
35.73	0.471	1.842	0.456	1.661
30.93	0.475	1.858	0.446	1.603
27.22	0.470	1.866	0.452	1.570
18.71	0.469	1.842	0.450	1.533
18.23	0.472	1.897	0.458	1.706
16.86	0.464	1.759	0.445	1.672
13.89	0.470	1.959	0.457	1.573
10.2	0.460	1.842	0.446	1.579
9.55	0.479	1.895	0.454	1.565
6.56	0.469	1.840	0.447	1.618
5.2	0.475	1.919	0.451	1.585
5	0.469	1.702	0.451	1.648
3.44	0.478	1.718	0.439	1.548
1.87	0.482	2.275	0.439	1.566

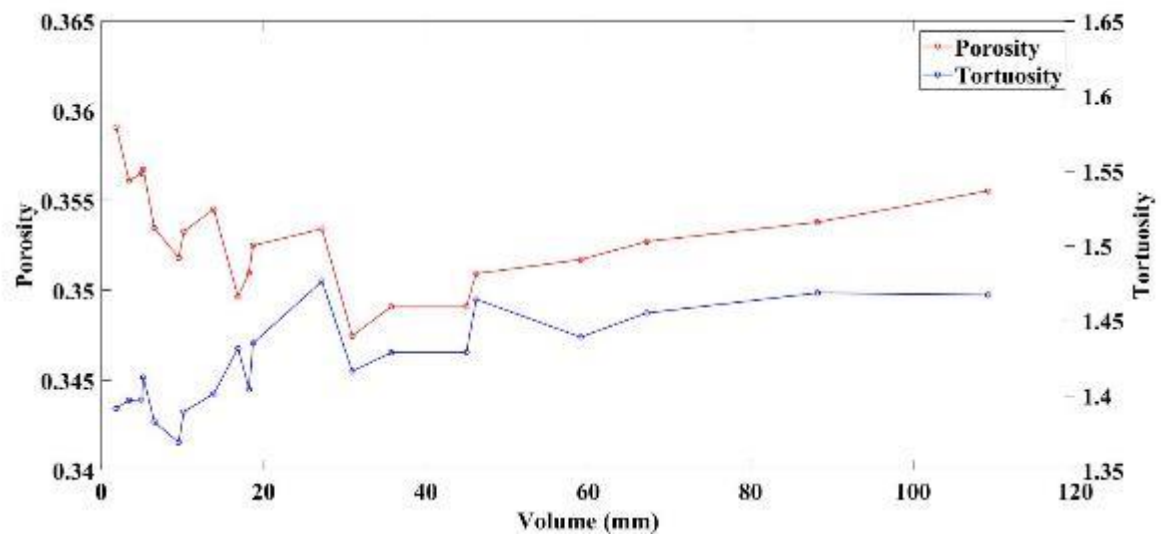
	System_13		System_14		System_15	
Volume (mm)	Porosity	Tortuosity	Porosity	Tortuosity	Porosity	Tortuosity
109.26	0.398	1.574	0.408	1.606	0.393	1.634
88.24	0.395	1.550	0.402	1.592	0.387	1.622
67.22	0.393	1.527	0.400	1.573	0.384	1.610
59.07	0.393	1.602	0.400	1.590	0.385	1.597
46.2	0.390	1.507	0.398	1.548	0.379	1.603
45	0.390	1.587	0.399	1.574	0.381	1.596
35.73	0.394	1.589	0.400	1.663	0.385	1.549
30.93	0.387	1.517	0.397	1.554	0.376	1.587
27.22	0.391	1.536	0.398	1.642	0.380	1.586
18.71	0.390	1.552	0.396	1.570	0.377	1.588
18.23	0.395	1.606	0.398	1.743	0.388	1.594
16.86	0.388	1.528	0.397	1.544	0.372	1.559
13.89	0.390	1.650	0.396	1.734	0.383	1.587
10.2	0.388	1.441	0.395	1.566	0.375	1.568
9.55	0.385	1.655	0.394	1.604	0.381	1.555
6.56	0.405	1.568	0.393	1.727	0.390	1.705
5.2	0.387	1.460	0.390	1.575	0.375	1.561
5	0.398	1.518	0.390	1.731	0.384	1.749
3.44	0.393	1.746	0.385	1.718	0.385	1.566
1.87	0.399	1.502	0.380	1.621	0.375	1.543

Appendix B: distribution curves for porosity and tortuosity

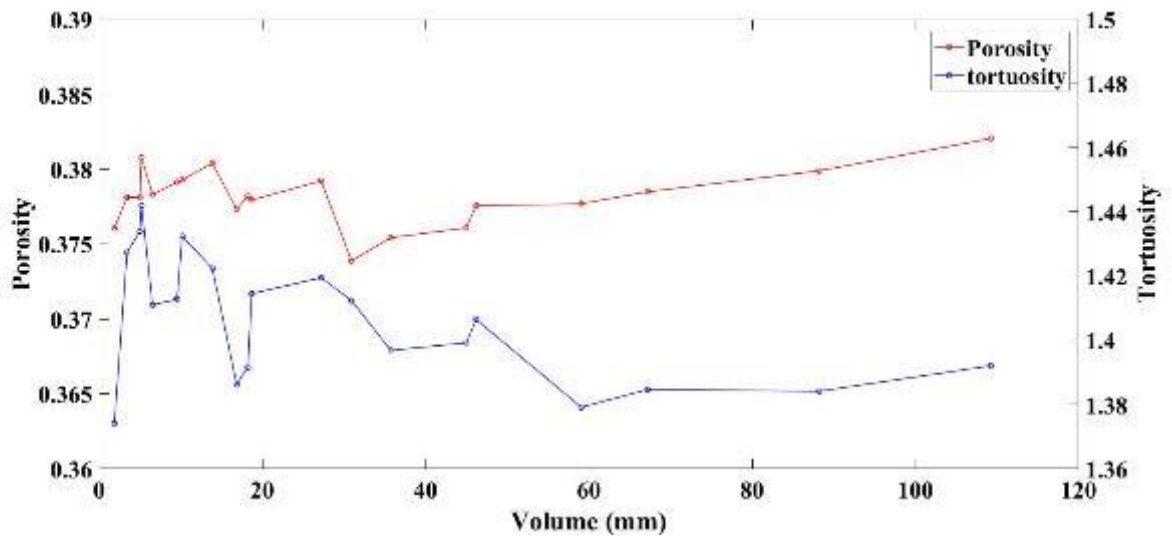
- System_1



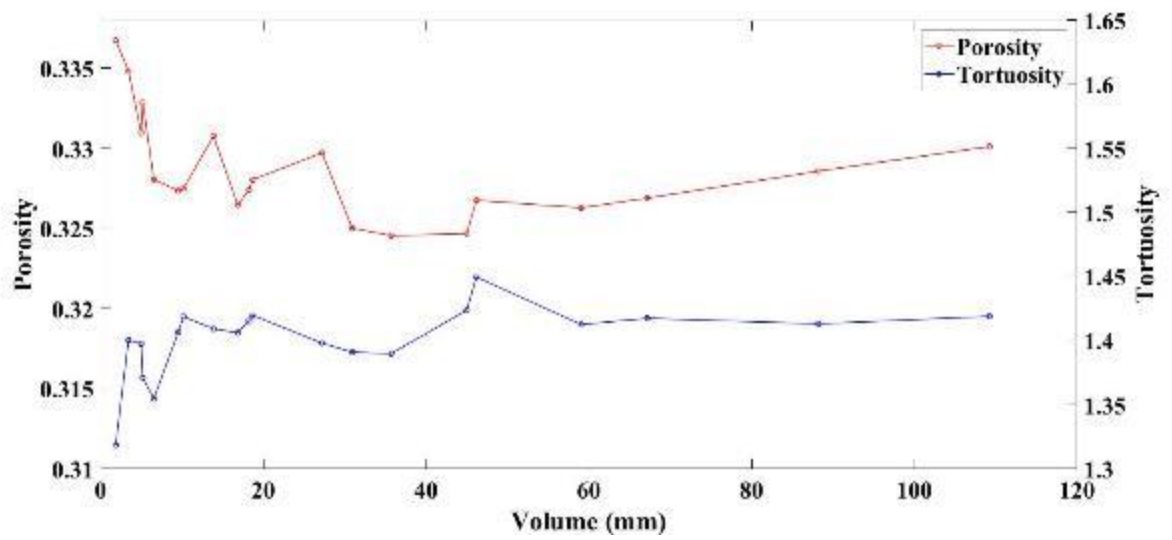
- System_2



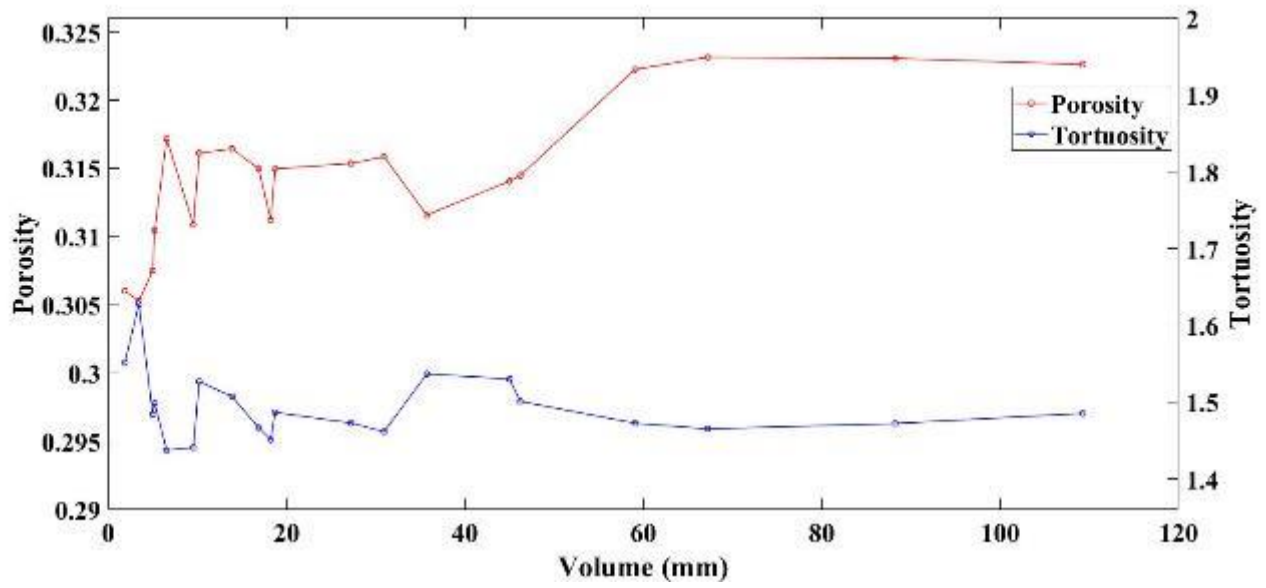
- System_3



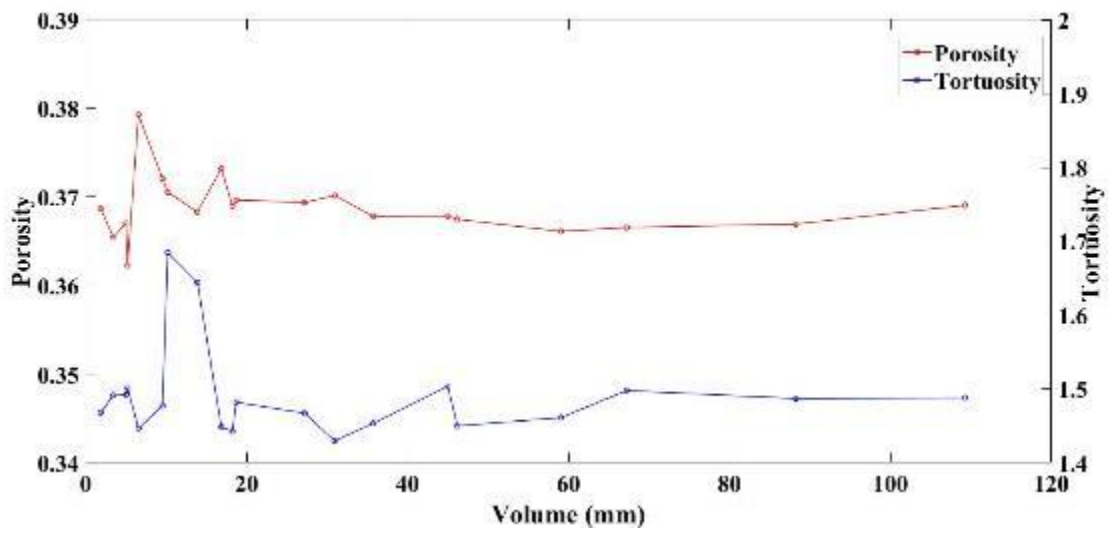
- System_4



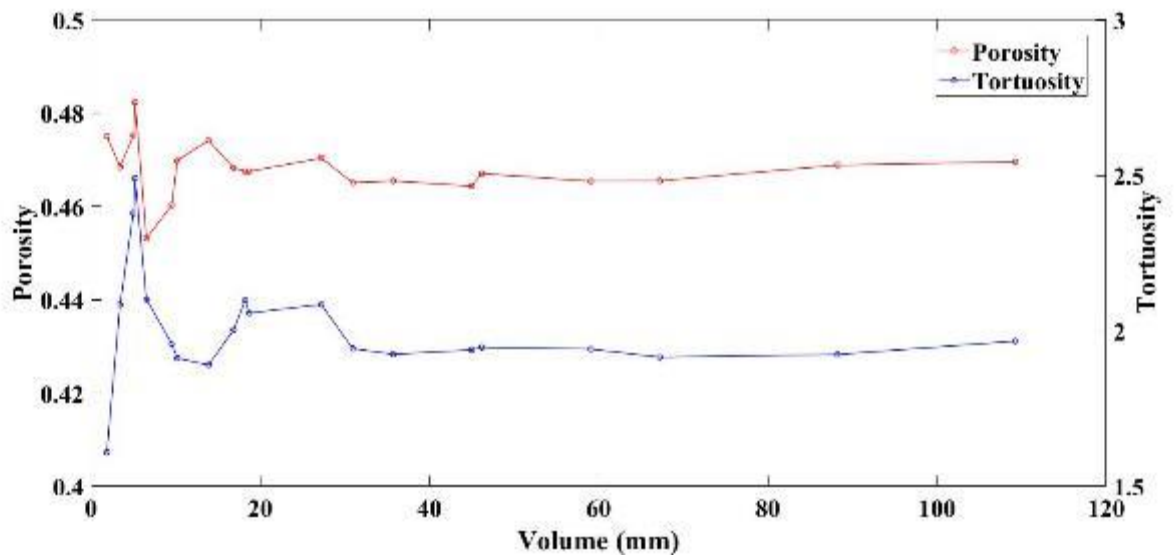
- System_5



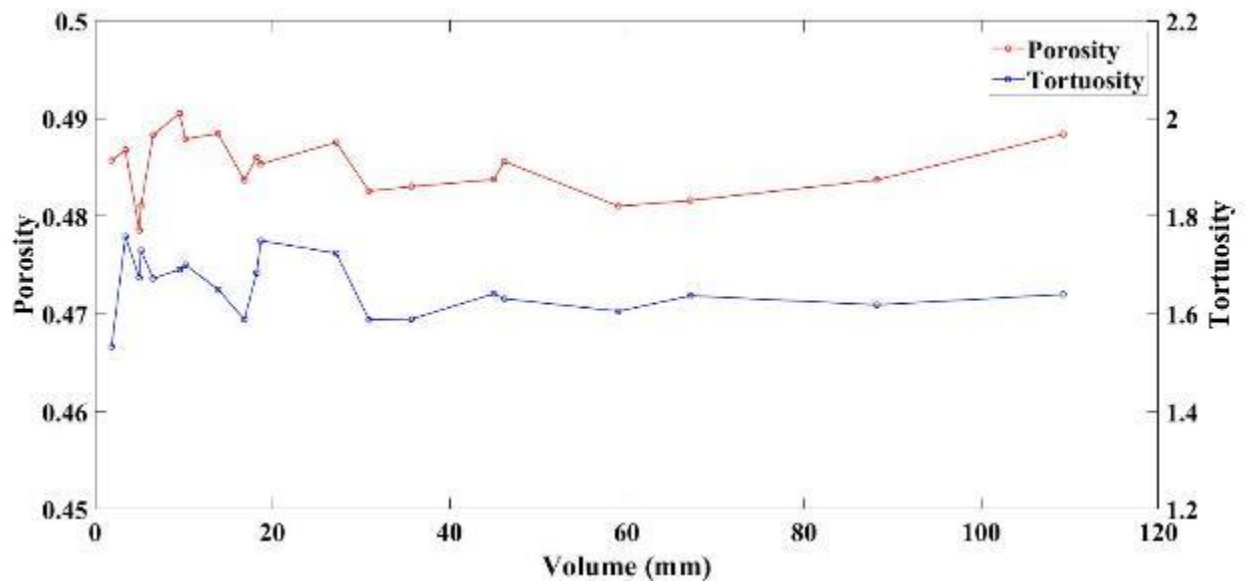
- System_6



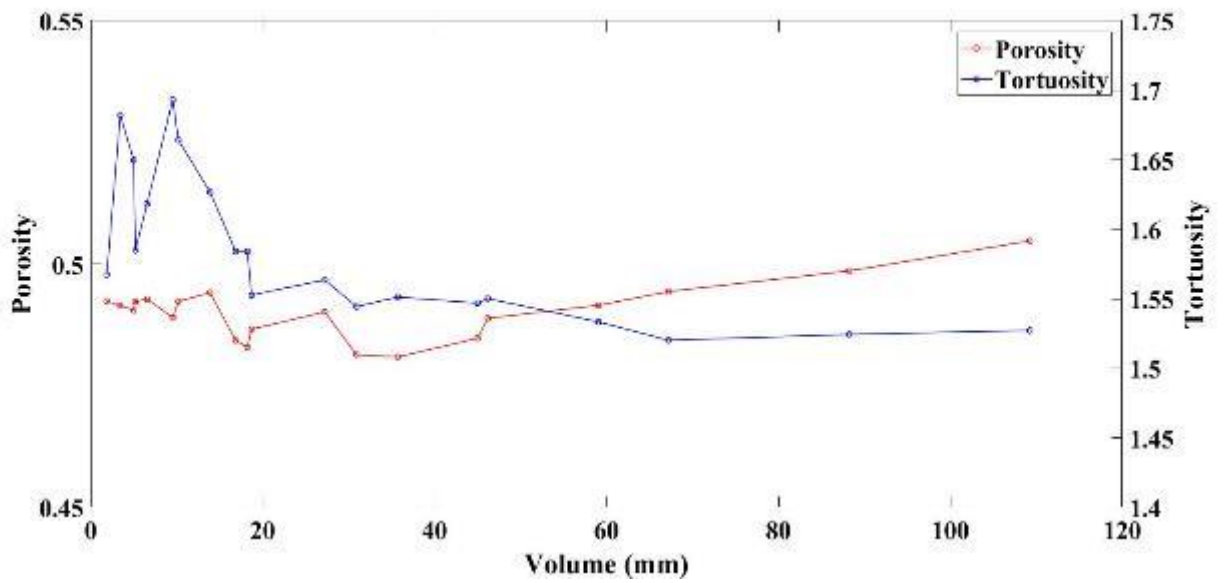
- System_7



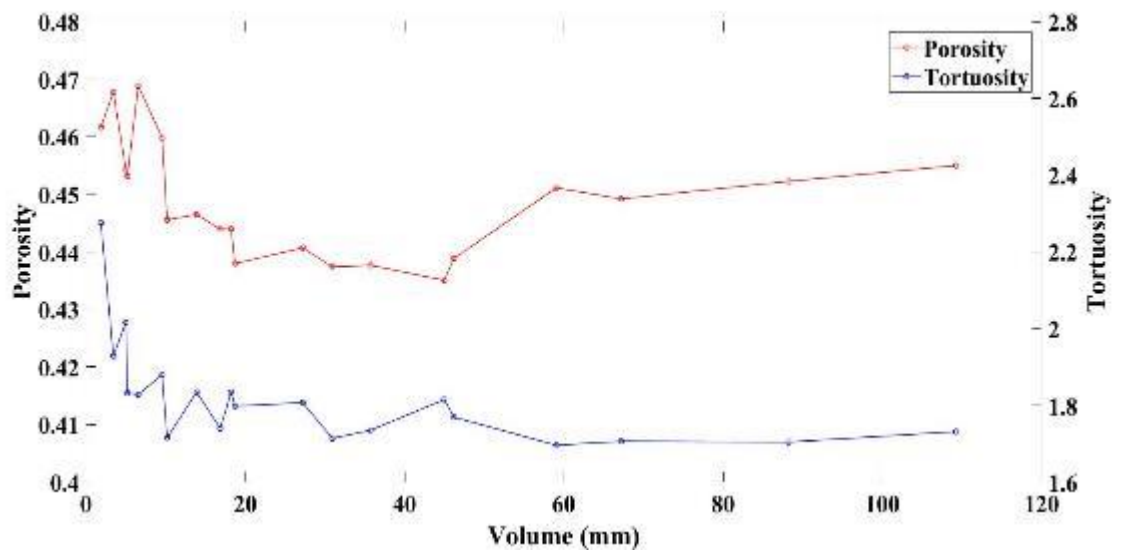
- System_8



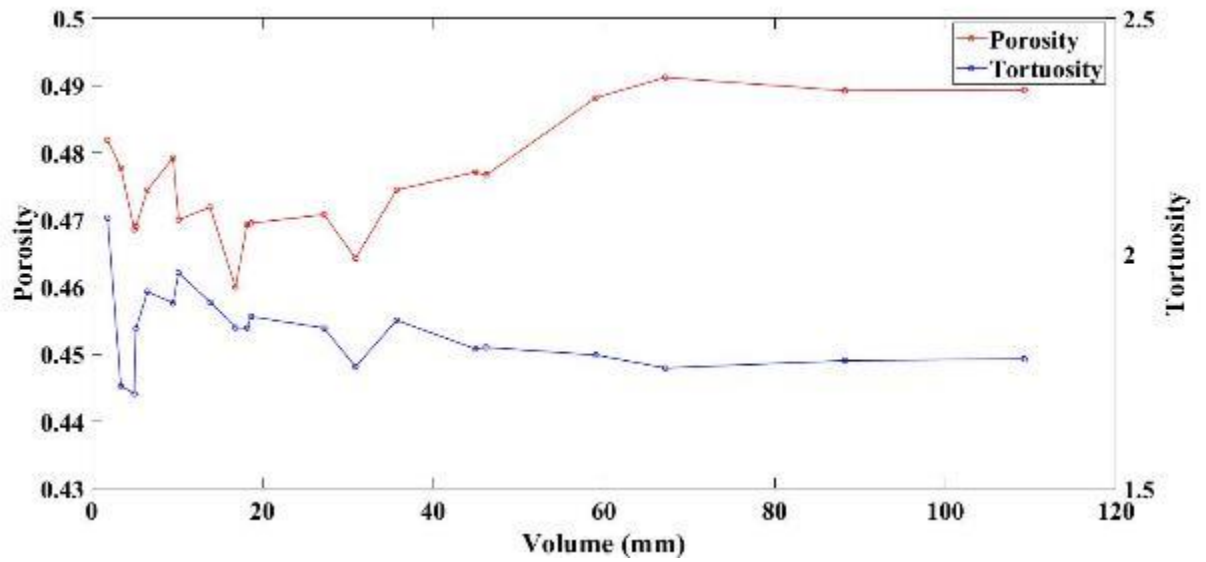
- System_9



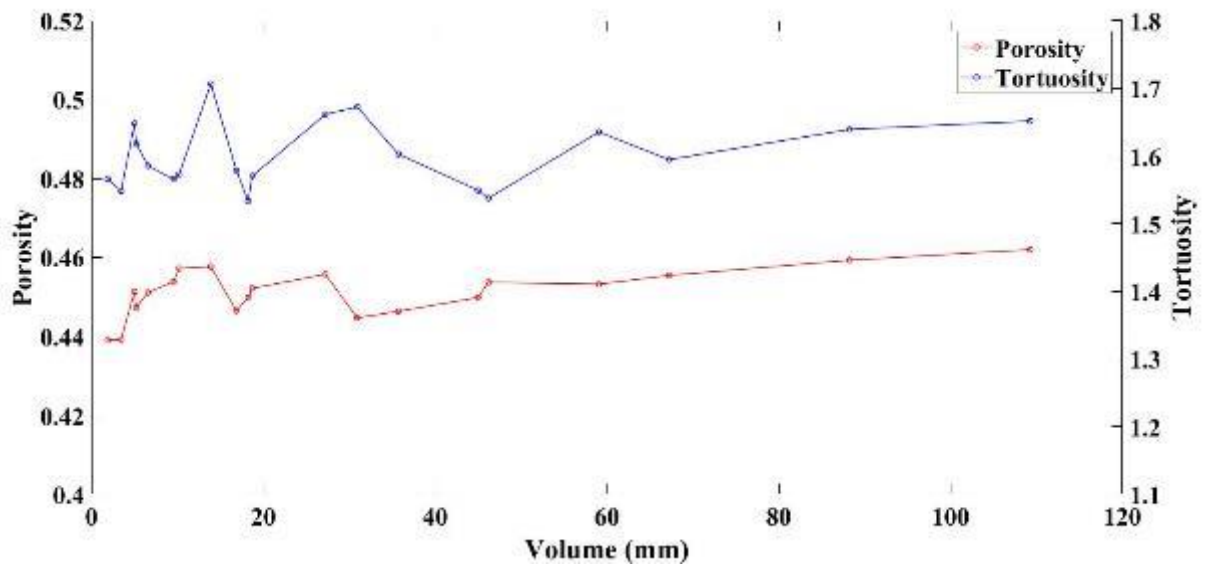
- System_10



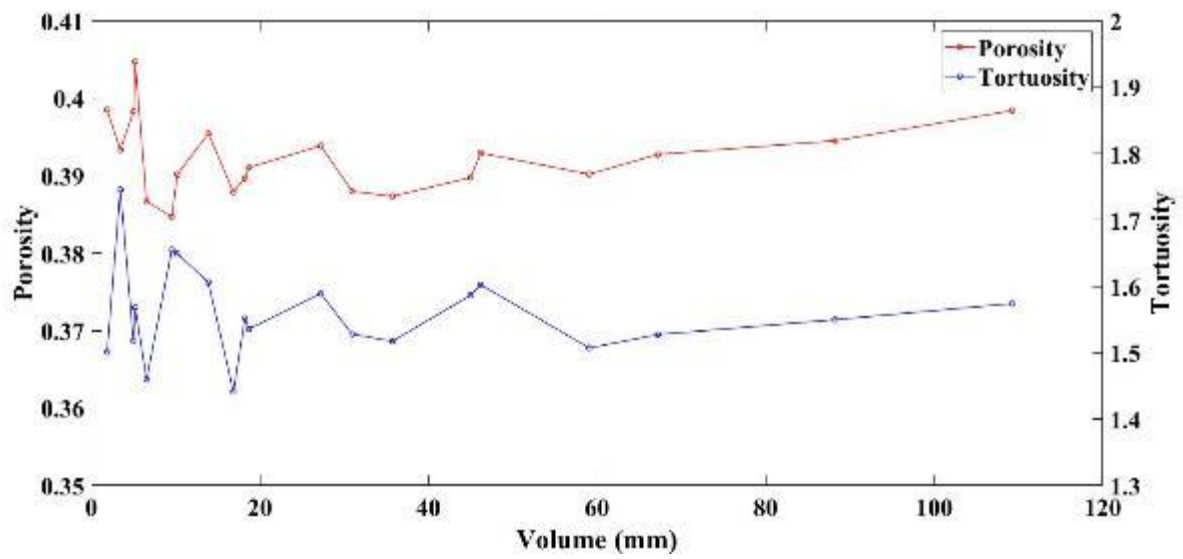
- System_11



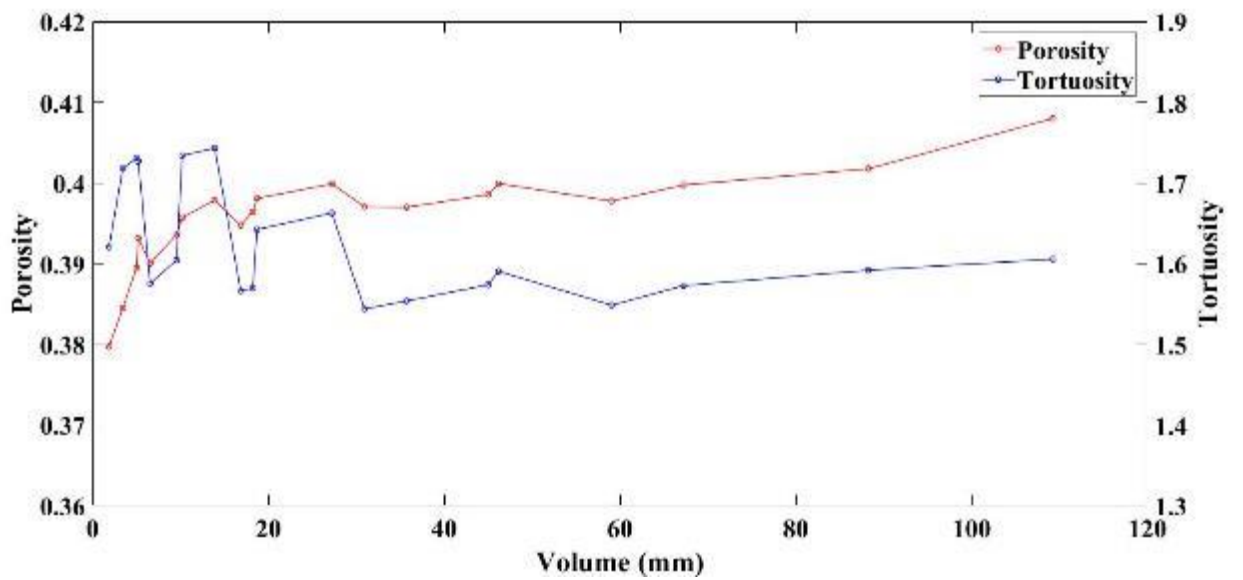
- System_12



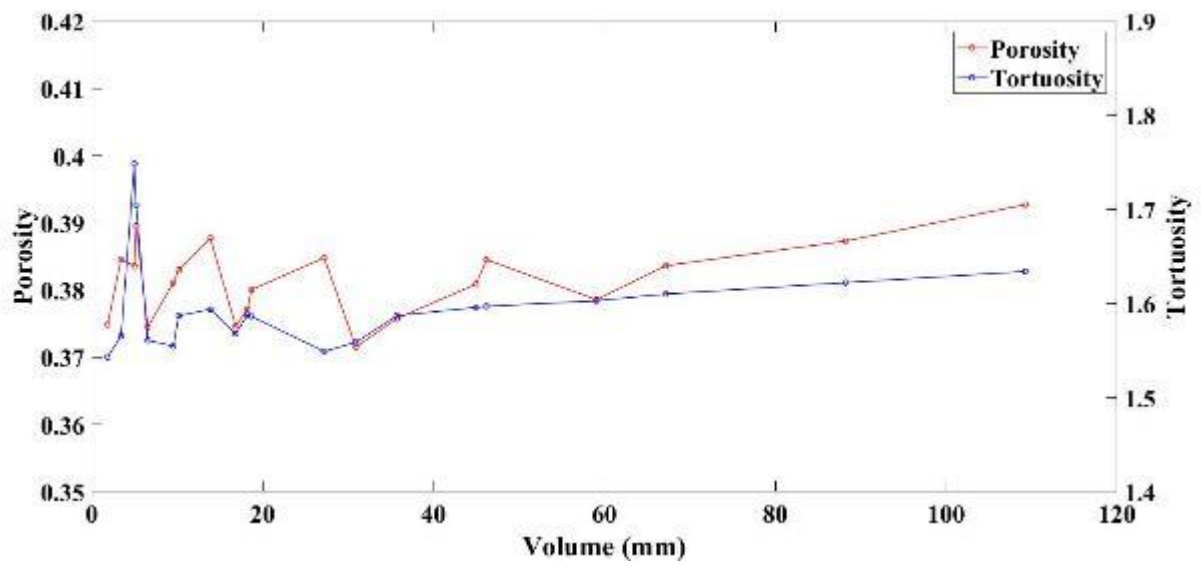
- System_13



- System_14



- System_15



Appendix C: REVmin Matlab code

```
load vol_n %%n is number of sub-volume (1-20)
t = 3.90*10^-10; %% set the tolerance for porosity
load poro_n
delta_poro_n=abs(poro_n(2:end)-poro_n(1:end-1));
delta_vol_n=abs(vol_n(2:end)-vol_n(1:end-1));
delta_poro_n_adj = delta_poro_n./delta_vol_n; %%
calculate the slope
REVP = find (delta_poro_n_adj<=t); %% compared with a
tolerance
n=size(REVP);
nREVP=[];
for i=2:n(1)
if REVP(i)-REVP(i-1)==1
    nREVP(i-1)=REVP(i-1);
end
end
x=nREVP(nREVP~=0);
REVminPp=vol_n(x(1));

tt = 2.02*10^-9; %% set the tolerance for tortousity
load tort_n
delta_tort_n=abs(tort_n(2:end)-tort_n(1:end-1));
delta_tort_n_adj = delta_tort_n./delta_vol_n;
REVT = find (delta_tort_n_adj<=tt);
n=size(REVT);
nREVT=[];
for i=2:n(1)
if REVT(i)-REVT(i-1)==1
    nREVT(i-1)=REVT(i-1);
end
end
y=nREVT(nREVT~=0);
REVminPt=vol_1(y(1));
if REVminPp==REVminPt
    fprintf('REV is %d',REVminPp)
end
```